Angular dependence and powder average of resonant inelastic x-ray scattering

Timothy G. Burrow,[1] Myrtille O. J. Y. Hunault,[1] Fabien Besnard,[2] Amélie Juhin,[3,*] and Christian Brouder[3]
[1]*Synchrotron SOLEIL, L'Orme des Merisiers, 91190 Saint-Aubin, France*
[2]*11 allée Hector Berlioz, 95230 Soisy-sous-Montmorency, France*
[3]*Institut de Minéralogie, de Physique des Matériaux et de Cosmochimie, IMPMC, UMR CNRS 7590, Sorbonne Université, Muséum National d'Histoire Naturelle, 75005 Paris, France*

(Received 28 October 2025; accepted 9 February 2026; published 16 March 2026)

Resonant inelastic x-ray scattering (RIXS) is a synchrotron-based spectroscopy that has seen growing interest across a range of scientific disciplines beyond fundamental physics. The interpretation of experimental RIXS data requires theoretical calculations based on the Kramers–Heisenberg formula. However, because of the dependence of RIXS on both the incident and scattered photon properties, a tractable treatment of the angular dependence in this formula has been lacking. In this work, within the electric-dipole approximation, we determine the number of fundamental spectra contributing to the RIXS cross section for all crystallographic point groups. We then derive a general expression for the RIXS cross section of isotropic samples such as untextured powders, homogeneous glasses or liquids, explicitly accounting for the polarization and propagation directions of both the incident and scattered photons. Simplified forms of the RIXS expressions are subsequently obtained for the most common point groups. Finally, we demonstrate the applicability of our formalism through two cases: $2p3d$ RIXS of Ni^{II} and the study of uranium $3d4f$ RIXS.

DOI: 10.1103/spng-p6c9

I. INTRODUCTION

Resonant inelastic x-ray scattering (RIXS) has proven to be extremely useful for investigating the properties of materials [1,2]. The richness of RIXS comes from the fact that it depends on the energy of the incident and scattered beams, as well as on the polarization and direction of the incident and scattered beams with respect to the sample, which allows access to additional spectral information [3–6]. To this end, instrumental capabilities have been implemented at synchrotron beamlines, providing the ability to control the polarization of the incident beam, vary the scattering angle, and perform polarization analysis of the scattered radiation [7–9].

While most of these studies are performed on single crystals, the number of studies on isotropic samples such as powders has been growing thanks to the application of RIXS by new scientific communities, e.g., chemistry [2,10], catalysis [11], high pressure [12], and actinide science [13]. These communities exploit RIXS to go beyond conventional x-ray absorption spectroscopy (XAS) through the use of high energy resolution fluorescence detection (HERFD). This approach, which involves taking a constant-emission-energy (CEE) cut in the RIXS plane, overcomes the limitations imposed by core-hole lifetime broadening and reveals otherwise hidden spectral features. A remarkable example is provided by the actinide M-edges, where the application of HERFD-XAS has reopened a very active field of investigation on these complex compounds [14,15]. However, the interpretation of experimental RIXS data often requires theoretical calculations. The Kramers-Heisenberg formula [16,17] has been implemented in various computational methods, from semi-empirical ligand field multiplet calculations [18] to more advanced *ab initio* calculations [19,20].

In a previous work [21], we investigated the dependence of RIXS on the polarization and direction of the incident and scattered beams of a sample without considering the effect of sample symmetry. We also derived explicit formulas for the polarization and angular dependence of an isotropic powder sample. However, the remaining challenge is that computational methods do not use an isotropic sample as input but the non-isotropic structural model of the system of interest (e.g., the point-group symmetry of the absorbing atom for semi-empirical multiplet calculations, a cluster around the absorber or the unit cell of a crystal for *ab initio* methods). In standard XAS computation, the spectra computed using the model system can easily be related to the experimental isotropic spectrum [22]. However, for RIXS, the coupling between the incident photon and the scattered photon makes this connection more challenging.

The purpose of this article is twofold. Firstly, we discuss the effect of a sample (molecular or crystal) symmetry on the angular and polarization dependencies, and secondly we determine the minimal number of calculations (or single-crystal measurements) required to compute these dependencies for an isotropic powder sample in the electric-dipole approximation for the incident and scattered beams. These derivations are performed in the impurity approximation, meaning that we neglect the interferences between the scattering events of different atoms. In the following, the coordinates (x, y, z) are in the standard orthonormal reference frame for point-group operations as defined by Altman and Herzig [23].

This paper is divided into six sections. In Sec. II, we demonstrate the well-known fact that the RIXS cross section

*Contact author: amelie.juhin@sorbonne-universite.fr

 ©2026 American Physical Society

for electric-dipole transitions is based on 81 spectra, and we prove that this number can be reduced further down to $n_G \leqslant 81$ fundamental spectra by taking symmetry into account. In Sec. III, we use spherical tensors to understand n_G and provide specific considerations about circular dichroism and site symmetry. In Sec. IV, we determine n_G and the relations between RIXS matrix elements for most symmetry groups as well as for the case of a spherically symmetric sample. In Sec. V, we derive the RIXS cross-section formula for a powder sample without taking the symmetry into account and then in Sec. VI, we give the RIXS cross-section formula for an isotropic sample knowing the symmetry of the absorber for most point groups. Finally, in Sec. VII, we draw some predictions for the experimental observations and we apply these formulas to selected examples to highlight the impact on the computed result for experiment predictions and theoretical similations.

II. RIXS CROSS SECTION AND SAMPLE SYMMETRY

The starting point of this analysis is the Kramers-Heisenberg formula [16,17] for RIXS

$$\frac{r_e^2}{m^2}\frac{\omega_s}{\omega}\sum_F\left|\sum_N \frac{\langle F|\epsilon_s^*\cdot\mathbf{p}e^{-i\mathbf{k}_s\cdot\mathbf{r}}|N\rangle\langle N|\epsilon\cdot\mathbf{p}e^{i\mathbf{k}\cdot\mathbf{r}}|I\rangle}{E_I-E_N+\hbar\omega+i\gamma}\right|^2 \times\delta(E_F+\hbar\omega_s-E_I-\hbar\omega),$$

where m is the electron mass, r_e is the classical electron radius, $r_e = e^2/(4\pi\epsilon_0 mc^2)$, $|I\rangle$, $|N\rangle$, $|F\rangle$ are the initial, intermediate, and final (possibly many-body) states, respectively, γ is the total width of the intermediate state $|N\rangle$, $\mathbf{p}$ and $\mathbf{r}$ are the momentum and position operators. The incident and scattered photons are characterized by the pulsation, wave vector and polarization vectors $\omega, \mathbf{k}, \epsilon$ and $\omega_s, \mathbf{k}_s, \epsilon_s$, respectively. Note that ϵ_s^* is the complex conjugate of ϵ_s.

In the present paper we limit ourselves to the RIXS cross section in the electric-dipole approximation [21],

$$\sigma(\epsilon_s,\epsilon) = \frac{r_e^2}{\hbar^2}\frac{\omega_s}{\omega}\sum_F\left|\sum_N \frac{(E_I-E_N)(E_N-E_F)}{E_I-E_N+\hbar\omega+i\gamma} \times\langle F|\epsilon_s^*\cdot\mathbf{r}|N\rangle\langle N|\epsilon\cdot\mathbf{r}|I\rangle\right|^2\delta_E, \tag{1}$$

where $\delta_E = \delta(E_F+\hbar\omega_s-E_I-\hbar\omega)$.

A. Group action

It will be convenient to use the concept of an action of a group on a set. Consider, for example, the group $G = O(3)$ of (linear) isometries, where an element g of G is represented by an orthogonal matrix g_{ij} (i.e., a rotation matrix possibly multiplied by an inversion). With g we can operate on: (i) a vector $\mathbf{r}$, (ii) a function $f(\mathbf{r})$, (iii) a quantum state $|\phi\rangle$, (iv) a sample s, etc.

In general, the action of an operation g on a set X is a transformation of any element x of X into an element y of X, denoted by $y = g\triangleright x$. In our examples: (i) X is the space $\mathbb{R}^3$ of three-dimensional vectors $\mathbf{r}$, (ii) X is the space of functions $f(\mathbf{r})$ on $\mathbb{R}^3$, (iii) X is the Hilbert space $\mathcal{H}$ of quantum states $|\phi\rangle$ of the system, (iv) X is the set S made of a sample s with all its possible orientations (note that we can rotate an object but we cannot mechanically invert it).

An action of a group G on a set X is a *group action* if the successive action of two arbitrary group elements is compatible with the group product, $g'\triangleright(g\triangleright x) = (g'\cdot g)\triangleright x$, where $g'\cdot g$ is the product in G, and if all elements x of X are stable under the action of the identity element e of G (i.e., $e\triangleright x = x$). In case (i), the action of an isometry g on a vector $\mathbf{r}$ is $g\triangleright\mathbf{r} = g\mathbf{r}$ (i.e., product of the matrix g_{ij} by the vector $\mathbf{r}$). In case (ii), the action of a rotation on a function $f(\mathbf{r})$ is [24]

$$(g\triangleright f)(\mathbf{r}) = f(g^{-1}\mathbf{r}), \tag{2}$$

where g^{-1}_{ij} is the inverse matrix of g_{ij}. For case (iii), we consider the action of an isometry on a quantum state that is an eigenstate of a Hamiltonian H with energy E. To take energy degeneracy into account, consider a basis $|\psi_1\rangle,\ldots,|\psi_n\rangle$ of the eigenstates of H with energy E. If G is a symmetry group of H (i.e., $g\triangleright H = H$ for all $g\in G$), we know that every element g of G transforms a state of H into a state with the same energy. More precisely, Wigner showed that there is a unitary matrix $U(g)$ such that [25]

$$g\triangleright|\psi_i\rangle = \sum_{j=1}^n U(g)_{ji}|\psi_j\rangle, \tag{3}$$

where $U(g)_{ji}$ is required instead of $U(g)_{ij}$ for $g\triangleright|\psi_i\rangle$ to be a (linear) group action,

$$\begin{aligned} g'\triangleright(g\triangleright|\psi_i\rangle) &= \sum_{j=1}^n U(g)_{ji}(g'\triangleright|\psi_j\rangle)\\ &= \sum_{j=1}^n\sum_{k=1}^n U(g)_{ji}U(g')_{kj}|\psi_k\rangle\\ &= \sum_{k=1}^n (U(g')U(g))_{ki}|\psi_k\rangle. \end{aligned}$$

This action is a group action if and only if $U(g')U(g) = U(g'\cdot g)$ [i.e., U is a unitary representation of G].

Consider now the projection onto the space of states of energy E,

$$P(E) = \sum_{j=1}^n |\psi_j\rangle\langle\psi_j|.$$

From the action of g on $|\psi_j\rangle$ of Eq. (3) and the unitarity of $U(g)$, we deduce that $P(E)$ is invariant under the action of g,

$$g\triangleright P(E) = \sum_{j,k,l} U(g)_{kj}|\psi_k\rangle\langle\psi_l|U(g)^*_{lj} = P(E). \tag{4}$$

These preliminaries enable us to calculate various actions of groups of isometries on the RIXS cross section.

B. Action of an isometry on the cross section

We calculate the action of isometries on the RIXS cross section in two ways: by acting on the states seen as a function of $\mathbf{r}$ as in Eq. (2) and then by acting on the states by a unitary representation as in Eq. (3).

We want to determine how the transition matrix element $\langle\phi|H_I|\psi\rangle = \int d\mathbf{r}\phi^*(\mathbf{r})\epsilon\cdot\mathbf{r}\psi(\mathbf{r})$ transforms under the action of a general isometry g. We show that

$$g\triangleright\langle\phi|H_I|\psi\rangle = \int d\mathbf{r}\phi^*(g^{-1}\mathbf{r})\epsilon\cdot\mathbf{r}\psi(g^{-1}\mathbf{r}). \tag{5}$$

This statement is not as trivial as it looks because the electric dipole form of H_I comes from a commutation of the original transition operator with the unperturbed Hamiltonian H_0 and we must check that it is not modified by the rotation of the sample in H_0.

First recall that the Hamiltonian of an electron in an electromagnetic field is $H = (\mathbf{p} - e\mathbf{a})^2/2m + V + ev$, where $\mathbf{p} = -i\hbar\nabla$, $\mathbf{a}$ is the vector potential and v the electric potential. Time-dependent perturbation theory for an incident electromagnetic wave described by the vector potential $\mathbf{a}\cos(\omega t)$ leads to the calculation of matrix elements such as $\langle\phi|H_I|\psi\rangle$, where $H_I = -e\mathbf{p}\cdot\mathbf{a}/m$ and $|\phi\rangle$ and $|\psi\rangle$ are eigenstates of $H_0 = \mathbf{p}^2/2m + V$ [22]. Within this model, acting with isometry g on the sample amounts to transforming the potential $V(\mathbf{r})$ into the potential $V'(\mathbf{r}) = (g\triangleright V)(\mathbf{r}) = V(g^{-1}\mathbf{r})$, as in Eq. (2). The Hamiltonian of the transformed sample in the original reference frame is $H_0' = \mathbf{p}^2/2m + V'$ and we go from the momentum transition operator $-e\mathbf{p}\cdot\mathbf{a}/m$ to the electric-dipole one by using $[\mathbf{r}, H_0] = [\mathbf{r}, H_0'] = (\hbar^2/m)\nabla$. Therefore, g does not act on the transition operator, which is still $\epsilon\cdot\mathbf{r}$.

To determine the eigenstates of H_0', we observe that a change of coordinates $\mathbf{r}\to\mathbf{r}' = g^{-1}\mathbf{r}$ transforms H_0 into $g\triangleright H_0 = (\mathbf{p}')^2/2m + V(\mathbf{r}')$, where $\mathbf{p}' = g^{-1}\mathbf{p}$. The orthogonality of g implies that $(\mathbf{p}')^2 = \mathbf{p}^2$ and $g\triangleright H_0 = H_0'$. Thus, the eigenstates of H_0' are the eigenstates of $g\triangleright H_0$, which are $\phi(\mathbf{r}') = \phi(g^{-1}\mathbf{r})$. This completes the proof of Eq. (5).

Note that the result is still valid if H_0 contains a two-body Coulomb interaction and in the presence of thermal vibrations if the experimental resolution is much larger than thermal energies [26]. It is also valid if the nonrelativistic Hamiltonian is replaced by a relativistic one, although the proof is more subtle, as shown in the Supplemental Material [27].

Starting from Eq (5), we change variables $\mathbf{r} = g\mathbf{r}'$ and notice that $d\mathbf{r} = d\mathbf{r}'$ (g being an orthogonal matrix, the Jacobian of the transformation is $|J| = |\det g| = 1$) to replace a transformation of the sample by a transformation of the transition operator and then a transformation of the polarization vector,

$$g\triangleright\langle\phi|\epsilon\cdot\mathbf{r}|\psi\rangle = \langle\phi|\epsilon\cdot(g\mathbf{r})|\psi\rangle = \langle\phi|(g^{-1}\epsilon)\cdot\mathbf{r}|\psi\rangle,$$

because g, as a linear isometry, conserves scalar products. The physical interpretation of this result is that the action of an isometry on a sample gives the same result as the action of the inverse isometry on the measurement device (represented by ϵ).

Thus, the action of an isometry g on the sample transforms the cross section into $g\triangleright\sigma(\epsilon_s,\epsilon) = \sigma(g^{-1}\epsilon_s, g^{-1}\epsilon)$ that it will be more convenient to write

$$g^{-1}\triangleright\sigma(\epsilon_s,\epsilon) = \sigma(g\epsilon_s, g\epsilon), \tag{6}$$

where we recall that we only assume g to be an isometry [i.e., an arbitrary element of $O(3)$] and not necessarily a symmetry of the sample. This property will be crucial in the following derivations. Note that Eq. (6) has no equivalent for antiunitary elements g of a magnetic group [28].

C. Action of a symmetry on the cross section

We consider now only isometries g, which are symmetries of the sample. By this we mean the point-group of the space group of a crystal or the point-group of a molecule. If the site of the absorbing atom has a lower symmetry group, then this subgroup must be used for the calculation of the spectrum, but the average over the different sites recovers the full point group [29].

For example, if the system is represented by the Hamiltonian $H_0 = \mathbf{p}^2/2m + V$, we assume that $(g\triangleright V)(\mathbf{r}) = V(g^{-1}\mathbf{r}) = V(\mathbf{r})$ and the action of g on the states of the system is described by Eq. (3).

To compute the action of g on $\sigma(\epsilon_s,\epsilon)$, we expand the modulus square in Eq. (1) for a given value of E_I, E_N, $E_{N'}$, and E_F [the presence of $E_{N'}$ being due to the fact that the sum over N is inside the modulus, as in Eq. (10)], and we replace the sum over states of energy E by a projector $P(E)$ to obtain terms of the type

$$T = \langle I|\epsilon^*\cdot\mathbf{r}P(E_{N'})\epsilon_s\cdot\mathbf{r}P(E_F)\epsilon_s^*\cdot\mathbf{r}P(E_N)\epsilon\cdot\mathbf{r}|I\rangle.$$

For simplicity, we considered a nondegenerate initial state $|I\rangle$. If it is degenerate, we must average over initial states (this also is how we take temperature effects into account) and T becomes

$$\frac{1}{n_I}\mathrm{Tr}(P(E_I)\epsilon^*\cdot\mathbf{r}P(E_{N'})\epsilon_s\cdot\mathbf{r}P(E_F)\epsilon_s^*\cdot\mathbf{r}P(E_N)\epsilon\cdot\mathbf{r}),$$

where n_I is the degeneracy of the initial state. By using the invariance of $P(E)$ under the action of a symmetry operation g [see Eq. (4)], we see that $g\triangleright T = T$, so that

$$g\triangleright\sigma(\epsilon_s,\epsilon) = \sigma(\epsilon_s,\epsilon). \tag{7}$$

Equations (6) and (7) lead us to the invariance

$$\sigma(\epsilon_s,\epsilon) = \sigma(g\epsilon_s, g\epsilon), \tag{8}$$

for every symmetry operation g of the sample. These symmetry operations form a group G. In other words, for any isometry of the absorbing atom point-group, the RIXS cross section is the same when the incident and scattered polarizations are rotated with this same operation.

D. Symmetry reduction of the cross section

To investigate the effect of symmetry on the RIXS cross section we rewrite its definition Eq. (1) as

$$\sigma(\epsilon_s,\epsilon) = \sum_{imjn}\epsilon_{si}^*\epsilon_m\epsilon_n^*\epsilon_{sj}a_{im,jn}, \tag{9}$$

where ϵ_m and ϵ_n run over the three Cartesian coordinates of ϵ and the same for ϵ_s, and

$$\begin{aligned} a_{im,jn} = \frac{r_e^2}{\hbar^2}\frac{\omega_s}{\omega}\sum_F\sum_{N,N'}\frac{(E_I - E_N)(E_N - E_F)}{E_I - E_N + \hbar\omega + i\gamma} \\ \times\frac{(E_I - E_{N'})(E_{N'} - E_F)}{E_I - E_{N'} + \hbar\omega - i\gamma}\langle F|r_i|N\rangle\langle N|r_m|I\rangle \\ \times\langle I|r_n|N'\rangle\langle N'|r_j|F\rangle\delta_E, \end{aligned} \tag{10}$$

where r_i, r_m, r_j, and r_n run over the Cartesian coordinates of $\mathbf{r}$. From this definition, we see that $a_{im,jn}$ is Hermitian (i.e., $a_{im,jn}^* = a_{jn,im}$), so that $a_{im,jn}$ has 81 components.

In the presence of nontrivial symmetry, relations exist between different $a_{im,jn}$ and we call *fundamental spectra* a set of real or imaginary parts of some $a_{im,jn}$ from which all nonzero $a_{im,jn}$ (and thus all RIXS spectra) can be computed. This is similar to the fundamental spectra defined by Thole and van der Laan for photoemission [30]. A specific $a_{im,jn}$ provides one fundamental spectrum if it is real or purely imaginary and two fundamental spectra if it has nonzero real and imaginary parts.

We shall see in Sec. V B that the invariance property of Eq. (8) implies

$$a_{im,jn} = \sum_{i'm'j'n'} N_{imjn,i'm'j'n'} a_{i'm',j'n'}, \tag{11}$$

where

$$N_{imjn,i'm'j'n'} = \frac{1}{|G|} \sum_{g\in G} g_{ii'} g_{mm'} g_{jj'} g_{nn'}. \tag{12}$$

In Sec. V B we prove that, thanks to the average of G in Eq. (12), the left-hand side of Eq. (11) has all the symmetries of the group G even if $a_{i'm',j'n'}$ has no symmetry. In other words, the invariance under G is entirely dependent on the properties of $N_{imjn,i'm'j'n'}$.

We give now the practical method to determine the symmetries of $a_{im,jn}$, which can easily be implemented with standard symbolic computing packages.

(i) Compute $N_{imjn,i'm'j'n'}$ by Eq. (12).

(ii) Transform $N_{imjn,i'm'j'n'}$ into a 81×81 matrix denoted by N^G. For this, associate a number k between 1 and 81 to each quadruple (i, m, j, n). For example $k = n + 3(j-1) + 9(m-1) + 27(i-1)$ and define $N^G_{kk'} = N_{imjn,i'm'j'n'}$.

(iii) Compute the number n_G of fundamental spectra of $a_{im,jn}$, which is the rank of N^G and also the trace of N^G since N^G is a projection [i.e., $(N^G)^2 = N^G$ and $(N^G)^\dagger = N^G$].

(iv) Gather in the rectangular matrix L^G the different nonzero lines of N^G (i.e., if the same line appears several times in N^G it appears only once in L^G). Let n_L be the number of lines of L^G (note that $n_L \geqslant n_G$).

(v) Compute the null space of the transpose of L^G, which gives you $n_L - n_G$ relations between lines by which you can write these lines in terms of n_G independent ones.

(vi) For each line L of L^G, identify the index k of the lines of N^G that are equal to L and transform back k into (i, m, j, n) to express this equality of lines as an equality between some $a_{im,jn}$.

In the Supplemental Material [27], we give N^G for the example of D_6, we show that the number of its nonzero lines is 21, the number of different nonzero lines of N^G is $n_L = 11$, there is one relation between lines and the rank of N^G is $n_G = 10$.

We can also determine the numbers n_{Re} and n_{Im} of nonzero real and imaginary fundamental spectra by noticing that the matrix P representing the permutation $(imjn) \to (jnim)$ commutes with N and satisfies $P^2 = 1$. From $Pa_{im,jn} = a_{jn,im} = a^*_{im,jn}$, we see that the number of independent real and imaginary parts in the tensor $a_{im,jn}$ are $n_{\mathrm{Re}} = \mathrm{Tr}((1+P)N/2)$ and $n_{\mathrm{Im}} = \mathrm{Tr}((1-P)N/2)$, respectively, with $n_{\mathrm{Re}} + n_{\mathrm{Im}} = n_G$.

TABLE I. Number of possibly nonzero matrix elements (i.e., that do not vanish by symmetry), number n_L of different matrix elements, number n_G of fundamental spectra and number n_{Im} of imaginary components for all crystallographic point groups, $SO(3)$ and $O(3)$. For an isotropic sample, n_S is the number of spectra needed to calculate the full angular dependence and n_C is the number of spectra needed to calculate the angular dependence when the polarization of the scattered beam is not measured, as explained in Sec. VI. The meaning of $\simeq$ is explained at the end of Sec. II D.

Point groups	$\neq 0$	n_L	n_G	n_{Im}	n_S	n_C
$C_1 \simeq C_i$	81	81	81	36	21	15
$C_2 \simeq C_s \simeq C_{2h}$	41	41	41	16	17	13
$D_2 \simeq C_{2v} \simeq D_{2h}$	21	21	21	6	15	12
$C_4 \simeq S_4 \simeq C_{4h}$	41	31	21	8	10	7
$D_4 \simeq C_{4v} \simeq D_{2d} \simeq D_{4h}$	21	11	11	2	9	7
$C_3 \simeq S_6$	73	47	27	12	11	7
$D_3 \simeq D_{3d}, C_{3v}$	37	19	14	4	8	6
$C_6 \simeq C_{3h} \simeq C_{6h}$	41	31	19	8	9	6
$D_6 \simeq C_{6v} \simeq D_{3h} \simeq D_{6h}$	21	11	10	2	8	6
$T \simeq T_h$	21	7	7	2	5	4
$O \simeq T_d \simeq O_h$	21	4	4	0	4	3
$SO(3) \simeq O(3)$	21	4	3	0	3	2

Table I gives for each crystallographic point-group, the number of matrix elements $a_{im,jn}$ that are not zero by symmetry, the number n_L of matrix elements that are different (in the sense that any matrix element is equal to one of those), and the number n_G of fundamental spectra (in the sense that any matrix element can be written as a linear combination of those). The symbol $\simeq$ in Table I means that, if the standard reference frame [23] is used (in particular the high symmetry axis is along the z axis), then all the matrix elements $a_{im,jn}$ of these two groups enjoy the same relations. The only difficulty comes from the case of C_{3v}, which has two usual reference frames [23]: the $1A$ parameters or the $1B$ parameters. With $1B$ parameters (where the mirror plane is perpendicular to the x axis), the matrix elements $a_{im,jn}$ have the same relations as those of C_{3v} and D_3 (see Sec. IV F). With $1A$ parameters (where the mirror plane is perpendicular to the y axis), the matrix elements have different relations (see Sec. IV G).

Several other examples will be given below.

III. ALTERNATIVE WAY TO THE FUNDAMENTAL SPECTRA

In this section we show that the number of fundamental spectra can be understood and obtained by hand using spherical tensors. We first define spherical parameters and then use them to calculate circular dichroism and to compute the average cross section over equivalent sites in a crystal or a molecule.

A. Definition of spherical parameters

Instead of fundamental spectra, we can define the *spherical parameters* S^{abc}_γ, which were defined in [21] by

$$S^{abc}_\gamma = \sum_{\alpha,\beta} \sum_{\mu\nu\mu'\nu'} (1\mu' 1\nu|a\alpha)(1\mu 1\nu'|b\beta)(a\alpha b\beta|c\gamma) \times A_{i\mu'} A_{m\nu} A_{n\mu} A_{j\nu'}\, a_{im,jn}, \tag{13}$$

where $(1\mu' 1\nu|a\alpha)$ are Clebsch-Gordan coefficients, A is the following 3×3 matrix relating Cartesian and spherical basis vectors,

$$\begin{pmatrix} e_x \\ e_y \\ e_z \end{pmatrix} = \begin{pmatrix} \frac{1}{\sqrt{2}} & 0 & -\frac{1}{\sqrt{2}} \\ \frac{i}{\sqrt{2}} & 0 & \frac{i}{\sqrt{2}} \\ 0 & 1 & 0 \end{pmatrix} \begin{pmatrix} e_{-1} \\ e_0 \\ e_{+1} \end{pmatrix}, \tag{14}$$

a and b take the values 0, 1, 2 and c runs from $|a-b|$ to $a+b$, so that c takes values from 0 to 4. Coefficient S_γ^{abc} is equal to $S_L^{g_1 g_2 a}$ of Ref. [21].

For the example of a sample with symmetry O, T_d, or O_h, the nonzero spherical parameters of this approach are

$$\begin{aligned} S_0^{000} &= a_{11,11} + 2a_{11,22}, \\ S_0^{110} &= -\sqrt{3}(a_{12,12} - a_{12,21}), \\ S_0^{220} &= \frac{1}{\sqrt{5}}(2a_{11,11} - 2a_{11,22} + 3a_{12,12} + 3a_{12,21}), \\ S_4^{224} &= S_{-4}^{224} = \sqrt{\frac{5}{14}}\, S_0^{224} \\ &= \frac{1}{2}(a_{11,11} - a_{11,22} - a_{12,12} - a_{12,21}). \end{aligned}$$

The relation between the components of the spherical tensor S^{224} is a well-known consequence of cubic symmetry [22]. It illustrates the fact that several spherical parameters S_γ^{abc} can be proportional. Of course, the number of independent spherical parameters is the same as the number of fundamental spectra.

The relation $a_{jn,im} = a_{im,jn}^*$ implies

$$\left(S_\gamma^{abc}\right)^* = (-1)^{a+b+c+\gamma} S_{-\gamma}^{abc},$$

which shows that S_0^{abc} is real if $a+b+c$ is even and purely imaginary if $a+b+c$ is odd.

To describe the action of an isometry g on the spherical parameters S_γ^{abc}, we first note that any isometry can be written $g = (-1)^{n_g} R$, where R is a rotation matrix and $n_g = 0$ or 1 if $\det g = 1$ (g is said to be even) or -1 (g is said to be odd), respectively. The rotation R will be called the *rotation part* of g.

The fact that the columns of matrix A can be considered as polarization vectors leads to the group action

$$g^{-1} \triangleright S_\gamma^{abc} = \sum_{\gamma'=-c}^{c} S_{\gamma'}^{abc} D_{\gamma'\gamma}^c(R),$$

where R is the rotation part of g and where $D_{\gamma'\gamma}^c(R)$ is the Wigner rotation matrix whose arguments are the same Euler angles as those of R. The part $(-1)^{n_g}$ of g disappears because the group action involves a product of four g.

When the symmetry group G is only made of even isometries, building group invariants from $a_{im,jn}$ reduces to building group invariants from spherical harmonics Y_c^γ and the number $n_G(c)$ of such invariants is given by the number of fully symmetric representations (denoted A_{1g} or A_1 or A) of G indicated in the section "Subduction from $O(3)$" of Altmann and Herzig's tables [23]. These group invariants can also be obtained explicitly by considering the group averages,

$$\langle Y_c^\gamma \rangle = \frac{1}{|G|} \sum_{g \in G} Y_c^{\gamma'} D_{\gamma'\gamma}^c(R).$$

These averages for $c = 2$ and 4 were constructed in Ref. [22].

Since a vector is also a spherical tensor of rank 1 (or a spherical harmonics for $\ell = 1$), we can represent the indices $imjn$ of $a_{im,jn}$ as the coupling of four spherical tensors of rank 1, that we denote $\mathbf{1}^{\otimes 4}$. The spherical tensor decomposition described by Eq. (13) can be obtained by the rules of angular momentum coupling,

$$\begin{aligned} \mathbf{1}^{\otimes 4} &= (\mathbf{1}^{\otimes 2})^{\otimes 2} = (\mathbf{0} \oplus \mathbf{1} \oplus \mathbf{2})^{\otimes 2} \\ &= (3\times\mathbf{0}) \oplus (6\times\mathbf{1}) \oplus (6\times\mathbf{2}) \oplus (3\times\mathbf{3}) \oplus \mathbf{4}, \end{aligned} \tag{15}$$

which means that $a_{im,jn}$ can be seen as the sum of three spherically symmetric tensors, six tensors of rank 1, six tensors of rank 2, three tensors of rank 3, and one tensor of rank 4. The total number of fundamental spectra is then the weighted sum of the numbers $n_G(c)$,

$$n_G = 3n_G(0) + 6n_G(1) + 6n_G(2) + 3n_G(3) + n_G(4).$$

The procedure must be modified when some elements g of G are odd, which is the case of the groups that are not in the first position in a line of Table I. Indeed, Altmann and Herzig's tables are constructed such that an inversion cancels all spherical tensors of odd rank, whereas it has no effect on the RIXS tensor. Therefore, these tables must be used with a group G' derived from G as follows. Since G contains an odd element, G can be written as the union of a set G^+ of even elements and a set G^- of odd elements. Since the inversion I commutes with all rotations and satisfies $I^2 = 1$, we see that G^+ is a subgroup of G and has the same number of elements as G^-. If I is an element of G^-, then $IG^- = G^+$, where IG^- is the set of $-g_{ij}$ with $g \in G^-$. In that case we take $G' = G^+$ [because the average Eq. (12) over G is the same as the average over G^+]. If I is not an element of G^-, then $G' = G^+ \cup IG^-$ is a group without odd elements, which has the same number of elements as G and such that G^+ is a subgroup of G'. The number n_G of fundamental spectra of G is then the weighted sum of $n_{G'}(c)$. In Table I, the first group of each line is the G' for all groups of that line.

Conversely, if the spherical parameters are constructed as linear combinations of Y_c^γ for all c such that $n_{G'}(c) \neq 0$, they can be transformed into relations for $a_{im,jn}$ by inverting Eq. (13),

$$\begin{aligned} a_{im,jn} = \sum_{a\alpha b\beta c\gamma} \sum_{\mu\nu\mu'\nu'} &(1\mu' 1\nu|a\alpha)(1\mu 1\nu'|b\beta)(a\alpha b\beta|c\gamma) \\ &\times A_{i\mu'}^* A_{m\nu}^* A_{n\mu}^* A_{j\nu'}^* S_\gamma^{abc}. \end{aligned} \tag{16}$$

B. Circular dichroism and permutation symmetry

Circular dichroism is the difference between the spectra obtained from left- and right-polarized incident beams. This is now a well-established technique [28,31–34].

Circular dichroism in RIXS measures the difference

$$\Delta\sigma(\epsilon_s, \epsilon) = \sigma(\epsilon_s, \epsilon) - \sigma(\epsilon_s, \epsilon^*). \tag{17}$$

By Eq. (9) we see that

$$\Delta\sigma(\epsilon_s,\epsilon) = \sum_{imjn} \epsilon^*_{si}\epsilon_m\epsilon^*_n\epsilon_{sj}(a_{im,jn} - a_{in,jm}).$$

Circular dichroism is usually normalized with respect to the average of $\sigma(\epsilon_s,\epsilon)$ and $\sigma(\epsilon_s,\epsilon^*)$, which is obtained by $(a_{im,jn} + a_{in,jm})/2$. The basic remark of this section is to notice that $a_{in,jm}$ is obtained from $a_{im,jn}$ by the permutation $(imjn) \to (injm)$.

We saw by Eq. (16) that

$$a_{im,jn} = \sum_{abc\gamma} Y^{ab}_{imjn}(c,\gamma)S^{abc}_{\gamma},$$

where

$$Y^{ab}_{imjn}(c,\gamma) = \sum_{\alpha\beta}\sum_{\mu\nu\mu'\nu'} (1\mu' 1\nu|a\alpha)(1\mu 1\nu'|b\beta)(a\alpha b\beta|c\gamma) \times A^*_{i\mu'}A^*_{m\nu}A^*_{n\mu}A^*_{j\nu'}.$$

The determination of circular dichroism in RIXS by $a_{im,jn} - a_{in,jm}$ amounts to the calculation of $Y^{ab}_{imjn}(c,\gamma) - Y^{ab}_{injm}(c,\gamma)$. The quantity $Y^{ab}_{injm}(c,\gamma)$ is obtained from $Y^{ab}_{imjn}(c,\gamma)$ by the permutation $(imjn) \to (injm)$. Spherical tensor recoupling techniques allow us to write this permutation in terms of $9j$-symbols [35], p. 70]

$$Y^{ab}_{injm}(c,\gamma) = \sum_{d,e} \Pi_{abde} \begin{Bmatrix} 1 & 1 & a \\ 1 & 1 & b \\ d & e & c \end{Bmatrix} Y^{de}_{imjn}(c,\gamma),$$

where

$$\Pi_{abde} = \sqrt{(2a+1)(2b+1)(2d+1)(2e+1)}.$$

To describe the sum over d, e, recall that Eq. (15) describes the multiplicity of rank c in the tensor decomposition of $\mathbf{1}^{\otimes 4}$. This multiplicity is $T(c) = 3, 6, 6, 3, 1$ for $c = 0, 1, 2, 3, 4$, respectively, where $T(c)$ is the number of pairs (a, b), a and b taking values in $\{0, 1, 2\}$, such that the triangle rule $|a - b| \leqslant c \leqslant a + b$ is satisfied. For example, for $c = 2$, the six pairs are $(a, b) = (0, 2), (1, 1), (1, 2), (2, 0), (2, 1), (2, 2)$. The sum over d, e is the sum over these $T(c)$ pairs.

Other permutations have a physical meaning: The measurement of the circular dichroism of the scattered beam is obtained by the permutation $(imjn) \to (jmin)$, the interchange of the incident and scattered beam is described by the permutation $(imjn) \to (njmi)$, which can be obtained by combining the permutations

$$Y^{ab}_{jnim}(c,\gamma) = (-1)^c Y^{ab}_{imjn}(c,\gamma),$$
$$Y^{ab}_{mijn}(c,\gamma) = (-1)^a Y^{ab}_{imjn}(c,\gamma),$$
$$Y^{ab}_{imnj}(c,\gamma) = (-1)^b Y^{ab}_{imjn}(c,\gamma).$$

In conclusion, every permutation of $(imjn)$ in $Y^{ab}_{imjn}(c,\gamma)$ can be expressed as a linear combination of $Y^{de}_{imjn}(c,\gamma)$. In group theoretical parlance, for each $c = 0, \ldots, 4$, the spherical tensors $Y^{ab}_{imjn}(c,\gamma)$ form a $T(c)$-dimensional representation of the symmetric group S_4 of permutations of four elements. The decomposition of these $T(c)$ tensors into irreducible representations of S_4 allows us to pick up the permutation symmetry required for the physical quantity of interest (circular dichroism of the incident or scattered beam, average spectrum of the incident or scattered beam, etc.).

Recall that S_4 is a group of order 24 with five irreducible representations: two of them are one dimensional [the trivial representation denoted by (4) and the sign representation denoted by (1,1,1,1)], one is two-dimensional [denoted by (2,2)] and two are three-dimensional [the standard representation denoted by (3,1) and the product of the sign and standard representations denoted by (2,1,1)]. An explicit calculation gives us the decomposition of $T(c)$-dimensional representation generated by $Y^{ab}(c)$ into irreducible representations of S_4,

$$3\times\mathbf{0} = (4) \oplus (2, 2),$$
$$6\times\mathbf{1} = (3, 1) \oplus (2, 1, 1),$$
$$6\times\mathbf{2} = (4) \oplus (3, 1) \oplus (2, 2),$$
$$3\times\mathbf{3} = (3, 1),$$
$$\mathbf{4} = (4).$$

This combination of point-group and permutation symmetries was also found useful in the calculation of Coulomb matrix elements [24].

The conclusion of this discussion is that all linear operations that are carried out on the 81 matrix elements of $a_{im,jn}$ can be encapsulated into equivalent linear operations on the (generally) much less numerous spherical parameters S^{abc}_{γ}.

A last useful relation is

$$Y^{ab}_{imjn}(c,\gamma)^* = (-1)^{c+\gamma} Y^{ab}_{imjn}(c,-\gamma).$$

C. From site to point-group symmetry

In general, the point symmetry group G of a molecule or crystal generates several equivalent sites. Consider a scattering atom at site A with coordinates $\mathbf{R}_A$. Its local symmetry group H is the set of elements g of G such that $g\mathbf{R}_A = \mathbf{R}_A$. The number of fundamental spectra for the RIXS of this atom is that of H. Since our formulation is independent of the translation between atoms, the scattering cross section of the full molecule or crystal is computed as the average of the cross sections of the equivalent atoms.

Here again, the use of spherical parameters will be convenient. The transition from site symmetry to point-group was discussed in detail for the case of x-ray absorption spectroscopy [29] and much of that discussion holds for RIXS. If $S^{abc}_{\gamma}(A)$ are the spherical parameters of site A, then the spherical parameters $S^{abc}_{\gamma}(B)$ corresponding to an equivalent site B obtained from A by the transformation $\mathbf{r}_B = g\mathbf{r}_A$ (plus a possible translation) where g is an element of G, which is not in H, are [29], Eq. (24)]

$$S^{abc}_{\gamma}(B) = \sum_{\gamma'=-c}^{c} S^{abc}_{\gamma'}(A)D^c_{\gamma'\gamma}(R^{-1}),$$

where R^{-1} is the inverse of the rotation part of g. And the spherical parameters of the full molecule or crystal is

$$S^{abc}_{\gamma} = \frac{1}{n}\sum_{g\in K}\sum_{\gamma'=-c}^{c} S^{abc}_{\gamma'}(A)D^c_{\gamma'\gamma}(R^{-1}), \qquad (18)$$

where K is a set of representatives of the coset of H in G, i.e., a set of elements of G that transform $\mathbf{r}_A$ into all the sites equivalent to A (up to possible translations), and n is the number of elements of K.

To illustrate the difference between the fundamental spectra and the spherical parameters approaches, consider a site with symmetry D_4 in a cubic crystal. We choose as coset representatives the identity, the rotation of $2\pi/3$ around the (111) axis and the rotation of $2\pi/3$ around the $(\bar{1}1\bar{1})$ axis, but the result does not depend on the representatives. The relation between the fundamental spectra of O and D_4 is

$$\begin{aligned}
a^{O}_{11,11} &= \tfrac{2}{3}a^{D_4}_{11,11} + \tfrac{1}{3}a^{D_4}_{33,33},\\
a^{O}_{11,22} &= \tfrac{1}{3}a^{D_4}_{11,22} + \tfrac{2}{3}\,\mathrm{Re}\left(a^{D_4}_{11,33}\right),\\
a^{O}_{12,12} &= \tfrac{1}{3}a^{D_4}_{12,12} + \tfrac{1}{3}a^{D_4}_{13,13} + \tfrac{1}{3}a^{D_4}_{31,31},\\
a^{O}_{12,21} &= \tfrac{1}{3}a^{D_4}_{12,21} + \tfrac{2}{3}\,\mathrm{Re}\left(a^{D_4}_{13,31}\right).
\end{aligned}$$

So we need to determine nine components (among the 11 of D_4) to build the four components of O. Only the imaginary parts of the fundamental spectra of D_4 are not required.

The spherical parameters for D_4 are three parameters $S_0^{aa0}(D_4)$ with $a = 0$, 1, and 2, six parameters $S_0^{ab2}(D_4)$ with $(ab) = (02)$, (11), (12), (20), (21), (22) and two parameters $S_0^{224}(D_4)$ and $S_4^{224}(D_4) = S_{-4}^{224}(D_4)$.

The spherical parameters of the crystal with symmetry O obtained from the average of Eq. (18) is then the three parameters $S_0^{aa0}(O) = S_0^{aa0}(D_4)$, which are the same as those of D_4 because a spherical tensor of rank 0 is invariant under rotation, the six parameters S_0^{ab2} vanish because no invariant of O can be constructed from $c = 2$ and we do not have to calculate them, and the nonzero spherical parameters are

$$\begin{aligned}
S_4^{224}(O) = S_{-4}^{224}(O) &= \sqrt{\frac{5}{14}}\,S_0^{224}(O)\\
&= \frac{5}{12}S_4^{224}(D_4) + \frac{\sqrt{70}}{24}S_0^{224}(D_4).
\end{aligned}$$

Therefore, we only have to calculate five spherical parameters of D_4 (instead of nine) to obtain the four spherical parameters of O.

IV. RIXS CROSS SECTION FOR VARIOUS POINT GROUPS

We give now the full determination of the fundamental spectra and of the relations between the $a_{im,jn}$, defined in Eq. (10), for most symmetry groups. Note that the nonzero $a_{im,jn}$ for all symmetry groups and the relations between them that do not involve $a_{im,jn} = a^*_{jn,im}$ can be found in Table E.22 of [36] or in the Bilbao Crystallographic Server [37], section Point-group symmetry/TENSOR, for Jahn's symbol $V4$. We give here additional information about their nature (real, imaginary, or mixed) and additional relations related to the Hermitian nature of $a_{im,jn}$.

A. Case C_1 or C_i

If the symmetry group is C_1 or C_i, no $a_{im,jn}$ is constrained to be zero by symmetry and the only relation between them is $a_{jn,im} = a^*_{im,jn}$, so that there are nine real fundamental spectra (i.e., $a_{im,im}$) and the other fundamental spectra can be grouped into 36 complex terms. The number of fundamental spectra is indeed

$$n_G = 3 \times 1 + 6 \times 3 + 6 \times 5 + 3 \times 7 + 9 = 81.$$

B. Case C_2, C_s or C_{2h}

If the symmetry group is C_2 or C_s, then $a_{im,jn}$ is zero if exactly one or exactly three of the indices $imjn$ are equal to 3. There are 16 terms where none of the indices $imjn$ are equal to 3, 24 terms where exactly two of the indices $imjn$ are equal to 3 and one term $imjn = 3333$. The only relation between matrix elements is $a_{jn,im} = a^*_{im,jn}$.

$$n_G = 3 \times 1 + 6 \times 1 + 6 \times 3 + 3 \times 3 + 5 = 41.$$

C. Case D_2 or C_{2v} or D_{2h}

If the symmetry group is D_2 or C_{2v} or D_{2h}, the matrix elements a_{imjn}, which are not zero by symmetry can be written as nine fundamental spectra ($a_{im,im}$ for i and m equal 1,2,3) that are always real and 12 ones that can be grouped into six complex parameters

$$\begin{aligned}
&a_{11,22} = a^*_{22,11}, \quad a_{11,33} = a^*_{33,11}, \quad a_{12,21} = a^*_{21,12},\\
&a_{22,33} = a^*_{33,22}, \quad a_{23,32} = a^*_{32,23}, \quad a_{13,31} = a^*_{31,13}.
\end{aligned}$$

$$n_G = 3 \times 1 + 6 \times 1 + 6 \times 3 + 3 \times 3 + 5 = 41.$$

D. Case C_4 or S_4 or C_{4h}

If the symmetry group is C_4 or S_4 or C_{4h}, we have seven real fundamental spectra

$$\begin{aligned}
&a_{13,13} = a_{23,23}, \quad a_{12,21} = a_{21,12},\\
&a_{12,12} = a_{21,21}, \quad a_{11,22} = a_{22,11},\\
&a_{11,11} = a_{22,22}, \quad a_{31,31} = a_{32,32}, \quad a_{33,33},
\end{aligned}$$

two imaginary fundamental spectra

$$a_{23,13} = -a_{13,23}, \quad a_{32,31} = -a_{31,32},$$

and six complex fundamental spectra

$$\begin{aligned}
a_{22,21} &= -a_{11,12} = a^*_{21,22} = -a^*_{12,11},\\
a_{22,12} &= -a_{11,21} = a^*_{12,22} = -a^*_{21,11},\\
a_{21,33} &= -a_{12,33} = a^*_{33,21} = -a^*_{33,12},\\
a_{23,31} &= -a_{13,32} = a^*_{31,23} = -a^*_{32,13},\\
a_{33,11} &= a_{33,22} = a^*_{11,33} = a^*_{22,33},\\
a_{31,13} &= a_{32,23} = a^*_{13,31} = a^*_{23,32}.
\end{aligned}$$

$$n_G = 3 \times 1 + 6 \times 1 + 6 \times 1 + 3 \times 1 + 3 = 21.$$

E. Case D_4 or C_{4v} or D_{2d} or D_{4h}

If the symmetry group is D_4 or C_{4v} or D_{2d} or D_{4h}, there are seven real fundamental spectra

$$\begin{aligned}
&a_{13,13} = a_{23,23}, \quad a_{31,31} = a_{32,32}, \quad a_{12,21} = a_{21,12},\\
&a_{12,12} = a_{21,21}, \quad a_{11,22} = a_{22,11}, \quad a_{11,11} = a_{22,22},\\
&a_{33,33},
\end{aligned}$$

and two complex parameters corresponding to four fundamental spectra

$$a_{13,31} = a_{23,32} = a^*_{31,13} = a^*_{32,23}$$
$$a_{11,33} = a_{22,33} = a^*_{33,22} = a^*_{33,11}.$$

$$n_G = 3 \times 1 + 6 \times 0 + 6 \times 1 + 3 \times 0 + 2 = 11.$$

F. Case D_3 or D_{3d} or C_{3v} with $1B$ reference frame

If the symmetry group is D_3 or D_{3d} or C_{3v} with $1B$ reference frame, the fundamental spectra are six real parameters

$$a_{13,13} = a_{23,23}, \quad a_{31,31} = a_{32,32}, \quad a_{12,21} = a_{21,12},$$
$$a_{12,12} = a_{21,21}, \quad a_{11,22} = a_{22,11}, \quad a_{33,33},$$

and four complex parameters

$$\begin{aligned} a_{11,32} &= a_{12,31} = a_{21,31} = -a_{22,32} \\ &= a^*_{31,12} = a^*_{31,21} = a^*_{32,11} = -a^*_{32,22}, \\ a_{11,23} &= a_{12,13} = a_{21,13} = -a_{22,23} \\ &= a^*_{13,12} = a^*_{13,21} = a^*_{23,11} = -a^*_{23,22}, \\ a_{11,33} &= a_{22,33} = a^*_{33,11} = a^*_{33,22}, \\ a_{13,31} &= a_{23,32} = a^*_{31,13} = a^*_{32,23}, \end{aligned}$$

with the remaining nonzero matrix elements

$$a_{11,11} = a_{22,22} = a_{11,22} + a_{12,12} + a_{12,21}.$$

$$n_G = 3 \times 1 + 6 \times 0 + 6 \times 1 + 3 \times 1 + 2 = 14.$$

G. Case C_{3v} with $1A$ reference frame

If the symmetry group is C_{3v} with $1A$ reference frame, the fundamental spectra are six real parameters

$$a_{13,13} = a_{23,23} \quad a_{31,31} = a_{32,32} \quad a_{12,21} = a_{21,12},$$
$$a_{12,12} = a_{21,21}, \quad a_{11,22} = a_{22,11}, \quad a_{33,33},$$

and four complex parameters

$$\begin{aligned} a_{12,23} &= a_{21,23} = a_{22,13} = -a_{11,13} \\ &= a^*_{13,22} = a^*_{23,12} = a^*_{23,21} = -a^*_{13,11}, \\ a_{12,32} &= a_{21,32} = a_{22,31} = -a_{11,31} \\ &= a^*_{31,22} = a^*_{32,12} = a^*_{32,21} = -a^*_{31,11}, \\ a_{33,11} &= a_{33,22} = a^*_{11,33} = a^*_{22,33}, \\ a_{31,13} &= a_{32,23} = a^*_{13,31} = a^*_{23,32}, \end{aligned}$$

with the remaining nonzero matrix elements

$$a_{11,11} = a_{22,22} = a_{11,22} + a_{12,12} + a_{12,21}.$$

$$n_G = 3 \times 1 + 6 \times 0 + 6 \times 1 + 3 \times 1 + 2 = 14.$$

H. Case C_6, C_{3h} and C_{6h}

The nonzero $a_{im,jn}$ of this case are the same as the ones of C_4, they satisfy the same relations as C_4 to which two relations are added

$$a_{11,11} = a_{22,22} = a_{11,22} + a_{12,12} + a_{12,21},$$
$$a_{11,12} + a_{12,11} = a_{12,22} + a_{22,12}.$$

The first one is a relation between real numbers. The second one is equivalent to the fact that the real parts of $a_{11,12}$ and $a_{12,22}$ are identical,

$$n_G = 3 \times 1 + 6 \times 1 + 6 \times 1 + 3 \times 1 + 1 = 19.$$

I. Case D_6, C_{6v}, D_{3h} and D_{6h}

If the symmetry group is D_6, C_{6v}, D_{3h}, or D_{6h}, we see from the decomposition of Eq. (15) that we have ten fundamental spectra (three coming from tensors of rank 0, six from tensors of rank 2 and 1 from the tensor of rank 4). The first six real ones are

$$a_{11,22} = a_{22,11}, \quad a_{12,12} = a_{21,21}, \quad a_{12,21} = a_{21,12},$$
$$a_{13,13} = a_{23,23}, \quad a_{31,31} = a_{32,32}, \quad a_{33,33}.$$

The other four are grouped into two complex parameters

$$a_{11,33} = a_{22,33} = a^*_{33,11} = a^*_{33,22},$$
$$a_{13,31} = a_{23,32} = a^*_{31,13} = a^*_{32,23}.$$

The remaining nonzero matrix elements $a_{im,jn}$ are

$$a_{11,11} = a_{22,22} = a_{11,22} + a_{12,12} + a_{12,21}.$$

$$n_G = 3 \times 1 + 6 \times 0 + 6 \times 1 + 3 \times 0 + 1 = 10.$$

J. Case T or T_h

If the symmetry group G is T or T_h, the explicit calculation of the matrix $N^G_{kk'}$ shows that there are 21 nonzero $a_{im,jn}$ that can be expressed in terms of seven fundamental spectra. Three of them are real

$$a_{11,11} = a_{22,22} = a_{33,33},$$
$$a_{12,12} = a_{23,23} = a_{31,31},$$
$$a_{13,13} = a_{21,21} = a_{32,32},$$

and the remaining four can be grouped into two complex numbers,

$$a_{11,22} = a_{22,33} = a_{33,11} = a^*_{11,33} = a^*_{22,11} = a^*_{33,22},$$
$$a_{12,21} = a_{23,32} = a_{31,13} = a^*_{13,31} = a^*_{21,12} = a^*_{32,23}.$$
$$n_G = 3 \times 1 + 6 \times 0 + 6 \times 0 + 3 \times 1 + 1 = 7.$$

K. Case O_h or O or T_d

If the symmetry group G is O_h or O or T_d, the explicit calculation of the matrix $N^G_{kk'}$ shows that there are 21 nonzero $a_{im,jn}$ that can be expressed in terms of four real fundamental spectra,

$$a_{11,11} = a_{22,22} = a_{33,33},$$
$$a_{11,22} = a_{11,33} = a_{22,33} = a_{22,11} = a_{33,11} = a_{33,22},$$
$$a_{12,12} = a_{13,13} = a_{23,23} = a_{21,21} = a_{31,31} = a_{32,32},$$
$$a_{12,21} = a_{13,31} = a_{23,32} = a_{21,12} = a_{31,13} = a_{32,23}.$$

They are real because, for instance, $a^*_{im,jn} = a_{jn,im}$ implies $a^*_{12,21} = a_{21,12} = a_{12,21}$.

$$n_G = 3 \times 1 + 6 \times 0 + 6 \times 0 + 3 \times 0 + 1 = 4.$$

An alternative mathematical approach to this question was proposed by Perla Azzi and colleagues [38] for the elastic tensor, which is also a fourth-rank tensor, but with a different symmetry with respect to the interchange of indices. They also define an interesting distance of a noncubic symmetry with respect to cubic symmetry.

L. a_{imjn} for spherical samples

For a spherical sample (e.g., an atom), we cannot use directly the average given by Eq. (12) because the number $|G|$ of rotations in infinite. However, since $SO(3)$ is a compact group, the average is obtained as a normalized integral over Euler angles α, β, and γ [39],

$$N_{imjn,i'm'j'n'} = \langle g_{ii'} g_{mm'} g_{jj'} g_{nn'} \rangle. \tag{19}$$

To compute this spherical average, we write each rotation matrix g in terms of the Wigner rotation matrix $D^1_{\mu\mu'}$, for which averages over angles are well known.

The relation giving the Cartesian basis (e_x, e_y, e_z) in terms of the spherical basis (e_{-1}, e_0, e_{+1}) is given by Eq. (14). Thus, the rotation matrix g is related to the Wigner rotation matrix D^1 by

$$g_{ij} = \sum_{\mu\mu'} A_{i\mu} A^*_{j\mu'} D^1_{\mu\mu'}. \tag{20}$$

This way, the spherical average of Eq. (19) is reduced to the angular average of a product of four Wigner matrices (implicitly) expressed in terms of Euler angles,

$$\begin{aligned} N' &= \left\langle D^1_{\mu_1,\mu'_1} D^1_{\mu_2,\mu'_2} D^1_{\mu_3,\mu'_3} D^1_{\mu_4,\mu'_4} \right\rangle \\ &= \frac{1}{8\pi^2} \int_0^{2\pi} d\alpha \int_0^{\pi} \sin\beta d\beta \int_0^{2\pi} d\gamma D^1_{\mu_1,\mu'_1} \\ &\quad \times D^1_{\mu_2,\mu'_2} D^1_{\mu_3,\mu'_3} D^1_{\mu_4,\mu'_4}. \end{aligned}$$

To compute this, we write the product of two Wigner matrices as a sum of Wigner matrices [35], p. 84] weighted by Clebsch-Gordan coefficients, then we use the angular average of a product of two Wigner matrices [35], p. 96] and obtain

$$\begin{aligned} N' = \sum_{b=0}^{2} \frac{(-1)^{\beta'-\beta}}{2b+1} &(1\mu_1, 1\mu_2|b\beta)(1\mu'_1, 1\mu'_2|b\beta') \\ &\times (1\mu_3, 1\mu_4|b-\beta)(1\mu'_3, 1\mu'_4|b-\beta'), \end{aligned}$$

where $\beta = \mu_1 + \mu_2 = -\mu_3 - \mu_4$ and similarly for β'. By multiplying with A and A^* and summing over μ_j, we find 21 nonzero $a_{im,jn}$ that can be expressed in terms of three fundamental spectra

$$\begin{aligned} a_{11,22} &= a_{11,33} = a_{22,33} = a_{22,11} = a_{33,11} = a_{33,22}, \\ a_{12,12} &= a_{13,13} = a_{23,23} = a_{21,21} = a_{31,31} = a_{32,32}, \\ a_{12,21} &= a_{13,31} = a_{23,32} = a_{21,12} = a_{31,13} = a_{32,23}. \end{aligned}$$

The remaining nonzero matrix elements are

$$a_{11,11} = a_{22,22} = a_{33,33} = a_{11,22} + a_{12,12} + a_{12,21}.$$

If we compare with a cubic sample, we see that the first fundamental spectrum of a cubic sample becomes the sum of the three other ones in the spherical case.

With these parameters, we recover the fact [21] that angular dependence of a RIXS spectrum of a powder is entirely determined by coefficients of $|\epsilon \cdot \epsilon_s|^2$ and $|\epsilon \cdot \epsilon_s^*|^2$.

If we put these coefficients $a_{im,jn}$ in the RIXS cross section of Eq. (9), we find that for general (i.e., possibly non normalized) ϵ and ϵ_s the RIXS cross section of a powder is

$$\begin{aligned} \sigma(\epsilon_s, \epsilon) = a_{11,22}|\epsilon \cdot \epsilon_s^*|^2 + a_{12,21}|\epsilon \cdot \epsilon_s|^2 \\ + a_{12,12}||\epsilon||^2||\epsilon_s||^2. \end{aligned} \tag{21}$$

This is a linear combination of the three possible spherically symmetric polynomials of degree four that can be constructed from two complex vectors ϵ and ϵ_s. For normalized polarization vectors, we recover the fact [21] that the angular dependence of a RIXS spectrum of a powder is determined by the coefficients of $|\epsilon \cdot \epsilon_s|^2$ and $|\epsilon \cdot \epsilon_s^*|^2$.

If the polarization of the scattered beam is not measured, we can average over its normalized polarizations perpendicular to the unit vector $\widehat{\mathbf{k}}_s$ along the scattered beam [21] to obtain

$$\begin{aligned} \sigma(\widehat{\mathbf{k}}_s, \epsilon) = \tfrac{1}{2}(a_{11,22} + 2a_{12,12} + a_{12,21})||\epsilon||^2 \\ - \tfrac{1}{2}(a_{11,22} + a_{12,21})|\epsilon \cdot \widehat{\mathbf{k}}_s|^2. \end{aligned} \tag{22}$$

V. RIXS MEASUREMENT OF A POWDER

In this section we deal in detail with the way RIXS measurements of an isotropic sample depend on the polarizations (and indirectly on the directions) of the incident and scattered beams.

For x-ray absorption spectra, it is well known that the spectrum $\langle \sigma_{\mathrm{XAS}} \rangle_{\mathrm{powder}}$ of a powder does not depend on polarization and can be calculated as the average of three spectra $\sigma_{\mathrm{XAS}}(\epsilon)$ calculated for a single crystal with a polarization vector ϵ along x, y, and z [40],

$$\langle \sigma_{\mathrm{XAS}} \rangle_{\mathrm{powder}} = \frac{\sigma_{\mathrm{XAS}}(\epsilon_x) + \sigma_{\mathrm{XAS}}(\epsilon_y) + \sigma_{\mathrm{XAS}}(\epsilon_z)}{3}.$$

Moreover, if the sample has cubic symmetry, then all three spectra are identical and only one spectrum must be computed to obtain $\langle \sigma_{\mathrm{XAS}} \rangle_{\mathrm{powder}} = \sigma_{\mathrm{XAS}}(\epsilon_x)$.

For a magnetic powder, the calculation of an x-ray absorption spectra needed a 302-point Lebedev quadrature [41]. For electron scattering spectra, the situation is more complex and an average over orientations required a 590-point Lebedev quadrature [42]. Moreover, a Lebedev quadrature averages a function $f(\theta, \phi)$ of the two angles θ and ϕ whereas we need to average spectra $f(\alpha, \beta, \gamma)$ depending on the three Euler angles that describe the orientation of the sample.

In this section, we write the RIXS spectrum of a powder as a weighted sum of RIXS spectra of a single crystal (or oriented molecule) with different incident and scattered polarizations. Since RIXS calculations can be computationally expensive, we look for the minimum number of such spectra wich turns out to be 21, and even of 15 spectra if the polarization state of the scattered beam is not measured. In the next section, we show that the symmetry of the sample further decreases this number.

A. Spherical tensor analysis

We know [21] that the polarization dependence of the RIXS cross section of an isotropic (e.g., powder) sample could entirely be described, in the electric-dipole approximation, by three parameters denoted S_0, S_1, and S_2, defined in Eq. (26) and related to $S_{L_0}^{gg0}$ of Ref. [21] by $S_g = \sqrt{2g+1}\, S^{gg0}$.

The general formula for arbitrary polarization of the incident beam and polarization detection of the scattered beam is

$$\sigma(\epsilon_s, \epsilon) = -\frac{S_1}{6} + \frac{S_2}{10} + \left(\frac{S_1}{6} + \frac{S_2}{10}\right)|\epsilon \cdot \epsilon_s|^2 + \left(\frac{S_0}{3} - \frac{S_2}{15}\right)|\epsilon \cdot \epsilon_s^*|^2. \tag{23}$$

We previously stressed [21] that the polarization ϵ_s of the scattered beam is characterized by the measurement device and several experimental setups were devised to explicitly measure the polarization of the scattered beam [43–47]. From the theoretical point of view [3,44], the crystal analyzers with (or without) explicit polarization detection can be considered as a polarization filter and when we say that the polarization is not measured, we mean that this filter gives the same weight to all polarization directions.

So, if the polarization of the scattered beam is not measured, the cross section becomes

$$\sigma(\widehat{\mathbf{k}}_s, \epsilon) = C_0 + C_1(|\epsilon \cdot \widehat{\mathbf{k}}_s|^2 - 1/3), \tag{24}$$

where $\widehat{\mathbf{k}}_s$ is the unit vector along the scattered beam and

$$C_0 = \frac{S_0}{9} - \frac{S_1}{9} + \frac{S_2}{9}, \quad C_1 = -\frac{S_0}{6} - \frac{S_1}{12} - \frac{S_2}{60}. \tag{25}$$

The term $-1/3$ in Eq. (24) is used to isolate C_0, which is the RIXS cross section when all scattered beams are collected [21]. In other words, C_0 is the RIXS cross section that would be measured with a detector (emission spectrometer) that would cover all directions in space.

The coefficients S_b are defined by

$$S_b = \sum_{imjn} X_{im,jn}(b) a_{im,jn}, \tag{26}$$

with

$$X_{im,jn}(b) = \sum_{\beta=-b}^{b} (-1)^{b-\beta} \sum_{\mu\nu\mu'\nu'} (1\mu' 1\nu | b\beta) \times (1\mu 1\nu' | b-\beta) A_{i\mu'} A_{m\nu} A_{n\mu} A_{j\nu'}, \tag{27}$$

where the matrix elements of A, defined in Eq. (14), appear because the original definition of $S_{L_0}^{bb0}$ in [21] was in terms of spherical components $\mathbf{r}_\mu^{(1)}$ and we work now with Cartesian components r_n. $X(b)$ is also related to the tensor of Sec. III B by $X(b) = \sqrt{2b+1}\, Y^{bb}(0,0)$. We changed the normalization to avoid the cluttering of square roots in formulas and tables, but $X(b)$ are no longer orthonormal for the Hilbert-Schmidt scalar product,

$$\sum_{imjn} X_{im,jn}(b) X^*_{im,jn}(b') = (2b+1)\delta_{bb'}. \tag{28}$$

Because of the definition of $X(b)$ as a coupling of spherical tensors, the matrix elements $X_{im,jn}(b)$ enjoy the same relations as $a_{im,jn}$ for a spherical sample (see Sec. IV L). In addition to the permutation symmetries discussed in Sec. III B, we note that each $X(b)$ is real-valued and the three tensors $X(b)$ commute in three ways,

$$\sum_{kl} X_{im,kl}(b) X_{kl,jn}(b') = \sum_{kl} X_{im,kl}(b') X_{kl,jn}(b),$$
$$\sum_{kl} X_{km,ln}(b) X_{km',ln'}(b') = \sum_{kl} X_{km,ln}(b') X_{km',ln'}(b),$$
$$\sum_{kl} X_{ik,jl}(b) X_{i'k,j'l}(b') = \sum_{kl} X_{ik,jl}(b') X_{i'k,j'l}(b),$$

and they are related to the spherical average of product of rotation matrices in Eq. (19) by

$$N_{imjn,i'm'j'n'} = \sum_{b=0}^{2} \frac{1}{2b+1} X_{im,nj}(b) X_{i'm',n'j'}(b),$$

which means that $X(b)$ are eigenstates of N for the eigenvalue 1, taking into account the normalization of Eq. (28).

We are now in a position to describe the problem at hand. We want to compute S_b for $b = 0, 1, 2$ and Eq. (26) suggests that, in the absence of symmetry, we need to determine the 81 fundamental spectra of $a_{im,jn}$. Moreover, some computer programs do not directly calculate $a_{im,jn}$, but cross-sections $\sigma(\epsilon_s, \epsilon)$ related to $a_{im,jn}$ by Eq. (9). Thus, we wish to find a certain number L of pairs of polarization vectors $(\epsilon_{sl}, \epsilon_l)$ such that

$$S_b = \sum_{l=1}^{L} \rho_l(b) \sigma(\epsilon_{sl}, \epsilon_l),$$

where $\rho_l(b)$ is the weight of $\sigma(\epsilon_{sl}, \epsilon_l)$ for S_b and we would like to minimize the number L of calculations.

As proved in Eq. (30), a generalization of the polarization identity requires 16 calculations of $\sigma(\epsilon_s, \epsilon)$ to calculate each $a_{im,jn}$. Therefore, a brute force approach would require $L = 16 \times 81 = 1296$ calculations of cross sections to compute the three parameters of the RIXS of a powder. We shall reduce this number to $L = 21$.

B. Generalized polarization identity

The polarization identity is a relation between

$$f(\mathbf{u}, \mathbf{v}) = \sum_{mn} u_m^* a_{mn} v_n,$$

where a_{mn} is a (finite dimensional) complex matrix, and $\phi(\mathbf{u}) = f(\mathbf{u}, \mathbf{u})$. Namely,

$$f(\mathbf{u}, \mathbf{v}) = \frac{1}{4} \sum_{k=0}^{3} (-i)^k \phi(\mathbf{u} + i^k \mathbf{v}).$$

Our case is more complicated because we must define

$$f(\mathbf{u}, \mathbf{u}'; \mathbf{v}, \mathbf{v}') = \sum_{imjn} u_i^* v_m^* a_{im,jn} u'_j v'_n, \tag{29}$$

and $\phi(\mathbf{u}, \mathbf{v}) = f(\mathbf{u}, \mathbf{u}; \mathbf{v}, \mathbf{v})$, so that $\sigma(\epsilon_s, \epsilon) = \phi(\epsilon_s, \epsilon^*)$. A lengthy but straightforward calculation proves the generalized

polarization identity that we need

$$f(\mathbf{u},\mathbf{u}';\mathbf{v},\mathbf{v}') = \frac{1}{16}\sum_{m=0}^{3}\sum_{n=0}^{3}(-i)^{m+n} \times \phi(\mathbf{u}+i^m\mathbf{u}';\mathbf{v}+i^n\mathbf{v}'). \tag{30}$$

An immediate consequence of this identity is that the invariance of the cross section (and therefore of ϕ) implies the invariance of f. Indeed, Eq. (8) implies

$$\begin{aligned}&\phi(g\mathbf{u}+i^m g\mathbf{u}';g\mathbf{v}'+i^n g\mathbf{v}')\\&=\phi(g(\mathbf{u}+i^m\mathbf{u}');g(\mathbf{v}'+i^n\mathbf{v}'))\\&=\phi(\mathbf{u}+i^m\mathbf{u}';\mathbf{v}'+i^n\mathbf{v}'),\end{aligned}$$

and then, by the polarization identity,

$$f(g\mathbf{u},g\mathbf{u}';g\mathbf{v},g\mathbf{v}') = f(\mathbf{u},\mathbf{u}';\mathbf{v},\mathbf{v}'), \tag{31}$$

for every g in the invariance group G of the sample. This identity extends the invariance of the function $\sigma(\epsilon_s,\epsilon)$ of two vectors ϵ_s and ϵ to the invariance of a function f of four vectors.

Similarly, Eq. (7) implies that, for any isometry g,

$$(g^{-1}\triangleright f)(\mathbf{u},\mathbf{u}';\mathbf{v},\mathbf{v}') = f(g\mathbf{u},g\mathbf{u}';g\mathbf{v},g\mathbf{v}'). \tag{32}$$

C. Symmetrization

We are now ready to prove that the left-hand side of Eq. (11) has all the symmetries of the group G even if $a_{i'm',j'n'}$ has no symmetry. More generally, we prove that, if f has no invariance whatsoever, then the average $\overline{f}$ defined by

$$\overline{f}(\mathbf{u},\mathbf{u}';\mathbf{v},\mathbf{v}') = \frac{1}{|G|}\sum_{g\in G} f(g\mathbf{u},g\mathbf{u}';g\mathbf{v},g\mathbf{v}'),$$

is invariant under any operation g of the invariance group G of the sample. This statement will be clear to the group theory experts, because the right-hand side is just the projection onto the fully symmetric representation of G, but let us show it. Let $h\in G$ be an element of the symmetry group. By linearity of the action,

$$(h^{-1}\triangleright\overline{f})(\mathbf{u},\mathbf{u}';\mathbf{v},\mathbf{v}') = \sum_{g\in G}\frac{(h^{-1}\triangleright f)(g\mathbf{u},g\mathbf{u}';g\mathbf{v},g\mathbf{v}')}{|G|}.$$

Now we can use Eq. (32), which is valid even if h is not a symmetry of f,

$$(h^{-1}\triangleright\overline{f})(\mathbf{u},\mathbf{u}';\mathbf{v},\mathbf{v}') = \sum_{g\in G}\frac{f(hg\mathbf{u},hg\mathbf{u}';hg\mathbf{v},hg\mathbf{v}')}{|G|}.$$

Any element g can be written in a unique way as $g=h^{-1}g'$ and g' runs over G when g runs over G. Thus,

$$\begin{aligned}(h^{-1}\triangleright\overline{f})(\mathbf{u},\mathbf{u}';\mathbf{v},\mathbf{v}') &= \sum_{g'\in G}\frac{f(g'\mathbf{u},g'\mathbf{u}';g'\mathbf{v},g'\mathbf{v}')}{|G|}\\&=\overline{f}(\mathbf{u},\mathbf{u}';\mathbf{v},\mathbf{v}').\end{aligned}$$

Since this is true for any $h\in G$, $\overline{f}$ is invariant under G even if f is not. Besides, if f is already invariant under G, then $\overline{f}=f$.

D. Singular-value decomposition

To decrease the number of calculations, we write a sort of singular-value decomposition of $X(b)$,

$$X_{im,jn}(b) = \sum_{k=1}^{9}\lambda^k(b)U^k_{ij}\left(V^k_{mn}\right)^*, \tag{33}$$

where it will turn out that the 3×3 matrices U^k and V^k do not depend on b. If we can diagonalize U^k and V^k as

$$\begin{aligned}U^k_{ij} &= \sum_{r=1}^{3}\mu^{kr}u^{kr}_i\left(u^{kr}_j\right)^*,\\V^k_{mn} &= \sum_{s=1}^{3}\nu^{ks}v^{ks}_m\left(v^{ks}_n\right)^*,\end{aligned}$$

we obtain by definition (26) of S_b,

$$S_b = \sum_{k,r,s}\lambda^k(b)\mu^{kr}\nu^{ks}\phi((\mathbf{u}^{kr})^*,\mathbf{v}^{ks}). \tag{34}$$

Equation (34) is already an improvement because the sum over k, r, s involves 81 cross sections $\phi((\mathbf{u}^{kr})^*,\mathbf{v}^{ks})$ instead of 1296, but further progress is possible.

To implement this singular-value decomposition, we define three 9×9 matrices $M(b)$ by $M(b)_{3(i-1)+j,3(m-1)+n} = X_{im,jn}(b)$,

$$M(0) = \frac{1}{3}\mathrm{Id}_9,$$

$$M(1) = \frac{1}{2}\begin{pmatrix}0&0&0&0&-1&0&0&0&-1\\0&0&0&1&0&0&0&0&0\\0&0&0&0&0&0&1&0&0\\0&1&0&0&0&0&0&0&0\\-1&0&0&0&0&0&0&0&-1\\0&0&0&0&0&0&0&1&0\\0&0&1&0&0&0&0&0&0\\0&0&0&0&0&1&0&0&0\\-1&0&0&0&-1&0&0&0&0\end{pmatrix},$$

and

$$M(2) = \frac{1}{6}\begin{pmatrix}4&0&0&0&3&0&0&0&3\\0&-2&0&3&0&0&0&0&0\\0&0&-2&0&0&0&3&0&0\\0&3&0&-2&0&0&0&0&0\\3&0&0&0&4&0&0&0&3\\0&0&0&0&0&-2&0&3&0\\0&0&3&0&0&0&-2&0&0\\0&0&0&0&0&3&0&-2&0\\3&0&0&0&3&0&0&0&4\end{pmatrix}.$$

These matrices commute and are real symmetric, so the singular-value decomposition turns out to be a diagonalization of $M(b)$ (this would not be the case if quadrupole transitions were taken into account) and a common set of real "eigenvectors" U^k and $V^k=U^k$ can be chosen for the three $X(b)$. Since all U^k are real, we can write

$$X_{im,jn}(b) = \sum_{krs}\lambda^k(b)\mu^{kr}\mu^{ks}u^{kr}_i u^{ks}_m\left(u^{kr}_j\right)^*\left(u^{ks}_n\right)^*.$$

TABLE II. Eigenvalues $\lambda^k(b)$ of $M(b)$ for $b = 0, 1, 2$ corresponding to their common eigenvectors U^k. The last line indicates whether U^k is symmetric (+) or antisymmetric (−).

b	U^1	U^2	U^3	U^4	U^5	U^6	U^7	U^8	U^9
0	$\frac{1}{3}$	$\frac{1}{3}$	$\frac{1}{3}$	$\frac{1}{3}$	$\frac{1}{3}$	$\frac{1}{3}$	$\frac{1}{3}$	$\frac{1}{3}$	$\frac{1}{3}$
1	-1	$-\frac{1}{2}$	$-\frac{1}{2}$	$-\frac{1}{2}$	$\frac{1}{2}$	$\frac{1}{2}$	$\frac{1}{2}$	$\frac{1}{2}$	$\frac{1}{2}$
2	$\frac{5}{3}$	$-\frac{5}{6}$	$-\frac{5}{6}$	$-\frac{5}{6}$	$\frac{1}{6}$	$\frac{1}{6}$	$\frac{1}{6}$	$\frac{1}{6}$	$\frac{1}{6}$
	+	−	−	−	+	+	+	+	+

We further observe in Table II that each U^k is either symmetric or antisymmetric, so the eigenvalues μ^{kr} for a given k are either all real or all purely imaginary and

$$X_{im,jn}(b) = \sum_{krs} \lambda^k(b)\mu^{kr}\mu^{ks}\left(u_i^{kr}\right)^*\left(u_m^{ks}\right)^* u_j^{kr}u_n^{ks}. \quad (35)$$

Thus,

$$S_b = \sum_{krs} \lambda^k(b)\mu^{kr}\mu^{ks}\phi(\mathbf{u}^{kr}, \mathbf{u}^{ks}).$$

The eigenvalues $\lambda^k(b)$ are given in Table II and the nine matrices U^k are

$$U^1 = \frac{1}{\sqrt{3}}\begin{pmatrix}1&0&0\\0&1&0\\0&0&1\end{pmatrix}, \quad U^2 = \frac{1}{\sqrt{2}}\begin{pmatrix}0&0&0\\0&0&-1\\0&1&0\end{pmatrix},$$

$$U^3 = \frac{1}{\sqrt{2}}\begin{pmatrix}0&0&-1\\0&0&0\\1&0&0\end{pmatrix}, \quad U^4 = \frac{1}{\sqrt{2}}\begin{pmatrix}0&-1&0\\1&0&0\\0&0&0\end{pmatrix},$$

$$U^5 = \frac{1}{\sqrt{2}}\begin{pmatrix}-1&0&0\\0&0&0\\0&0&1\end{pmatrix}, \quad U^6 = \frac{1}{\sqrt{2}}\begin{pmatrix}0&0&0\\0&0&1\\0&1&0\end{pmatrix},$$

$$U^7 = \frac{1}{\sqrt{2}}\begin{pmatrix}0&0&1\\0&0&0\\1&0&0\end{pmatrix}, \quad U^8 = \frac{1}{\sqrt{6}}\begin{pmatrix}-1&0&0\\0&2&0\\0&0&-1\end{pmatrix},$$

$$U^9 = \frac{1}{\sqrt{2}}\begin{pmatrix}0&1&0\\1&0&0\\0&0&0\end{pmatrix}.$$

Matrices U^k for $k = 1, 5$, and 8 are already diagonal, so we can take for eigenvectors $\mathbf{u}^{kr}$ (for $k = 1, 5$, and 8) the same real unit vectors $\mathbf{e}_x$, $\mathbf{e}_y$, and $\mathbf{e}_z$ along the x, y, and z axes, respectively. This means that we can calculate $k = 1, 5$, and 8 with the same nine values of $\phi(\mathbf{e}_p, \mathbf{e}_q)$, where p and q take the values x, y, and z, even if only four of them are useful for $k = 5$ because of its zero eigenvalue.

For $k = 2$, 3, and 4, each U^k is a real antisymmetric matrix, its two nonzero eigenvalues are $\mu^{kr} = \pm\imath/\sqrt{2}$, the corresponding eigenvectors are of the form $\mathbf{u}^{kr} = \boldsymbol{\pi}_{pq}^{\pm} = (\pm\imath\mathbf{e}_p + \mathbf{e}_q)/\sqrt{2}$ (i.e., $\boldsymbol{\pi}_{yz}^{\pm}$ for $k = 2$, $\boldsymbol{\pi}_{xz}^{\pm}$ for $k = 3$, $\boldsymbol{\pi}_{xy}^{\pm}$ for $k = 4$) and we have to calculate four different $\phi(\mathbf{u}^{kr}, \mathbf{u}^{ks})$ for each k.

For $k = 6$, 7, and 9, each U^k is a real symmetric matrix, its two nonzero eigenvalues are $\mu^{kr} = \pm 1/\sqrt{2}$, the corresponding eigenvectors are of the form $\mathbf{u}^{kr} = \mathbf{e}_{pq}^{\pm} = (\pm\mathbf{e}_p + \mathbf{e}_q)/\sqrt{2}$ (i.e., $\mathbf{e}_{yz}^{\pm}$ for $k = 6$, $\mathbf{e}_{xz}^{\pm}$ for $k = 7$, $\mathbf{e}_{xy}^{\pm}$ for $k = 9$) and we have again to calculate four different $\phi(\mathbf{u}^{kr}, \mathbf{u}^{ks})$ for each k.

Therefore, the total number of cross sections to calculate is reduced from 81 to $9 + 3 \times 4 + 3 \times 4 = 33$.

E. Further reduction

To proceed with the reduction, we define the fourth-rank tensors $(\mathbf{u}, \mathbf{v})$ with components

$$(\mathbf{u}, \mathbf{v})_{imjn} = u_i^* v_m^* u_j v_n,$$

and we write Eq. (35) in a more general form,

$$X_{im,jn}(b) = \sum_l \rho_l(b)(\mathbf{u}_l, \mathbf{v}_l)_{imjn}, \quad (36)$$

where l enumerates the krs indices, $(\mathbf{u}_l, \mathbf{v}_l)$ is a fourth-rank tensor and $\rho_l(b) \in \mathbb{R}$ is its weight. After reduction, Eq. (36) will still be valid whereas Eq. (35) will not.

By examining the 33 fourth-rank tensors in Eq. (35), we observe the following linear relations:

$$\sum_{r,s\in\{p,q\}} (\mathbf{e}_r, \mathbf{e}_s) = \sum_{\eta,\eta'\in\{+,-\}} \left(\boldsymbol{\pi}_{pq}^{\eta}, \boldsymbol{\pi}_{pq}^{\eta'}\right),$$

$$\sum_{r,s\in\{p,q\}} (\mathbf{e}_r, \mathbf{e}_s) = \sum_{\eta,\eta'\in\{+,-\}} \left(\mathbf{e}_{pq}^{\eta}, \mathbf{e}_{pq}^{\eta'}\right),$$

where $(p, q) = (y, z)$, (x, z), and (x, y). These six linear relations would enable us to remove six fourth-rank tensors $(\mathbf{u}_l, \mathbf{v}_l)$. However, we can further reduce them by observing that $(\mathbf{u}^+, \mathbf{u}^-)$ and $(\mathbf{u}^-, \mathbf{u}^+)$ always have the same weight in the calculation of $X(b)$ by Eq. (35) for any $\mathbf{u} = \boldsymbol{\pi}_{pq}$ and $\mathbf{u} = \mathbf{e}_{pq}$. Therefore, we can use

$$\sum_{\eta=\pm} \left(\boldsymbol{\pi}_{pq}^{\eta}, \boldsymbol{\pi}_{pq}^{-\eta}\right) = \sum_{r,s\in\{p,q\}} (\mathbf{e}_r, \mathbf{e}_s) - \sum_{\eta=\pm} \left(\boldsymbol{\pi}_{pq}^{\eta}, \boldsymbol{\pi}_{pq}^{\eta}\right),$$

$$\sum_{\eta=\pm} \left(\mathbf{e}_{pq}^{\eta}, \mathbf{e}_{pq}^{-\eta}\right) = \sum_{r,s\in\{p,q\}} (\mathbf{e}_r, \mathbf{e}_s) - \sum_{\eta=\pm} \left(\mathbf{e}_{pq}^{\eta}, \mathbf{e}_{pq}^{\eta}\right),$$

to remove 12 tensors $(\mathbf{u}_l, \mathbf{v}_l)$ instead of six and we are finally left with 21 fourth-rank tensors.

Our final result is

$$S_b = \sum_{l=1}^{21} \rho_l(b)\phi(\mathbf{u}_l, \mathbf{v}_l) = \sum_{l=1}^{21} \rho_l(b)\sigma(\mathbf{u}_l, \mathbf{v}_l^*), \quad (37)$$

for the tensors and the weights given in Table III.

We can also write C_0 and C_1 in the angular dependence of Eq. (24) directly in terms of 15 cross sections,

$$C_0 = \frac{1}{9}\sum_{pq} \sigma(\mathbf{e}_p, \mathbf{e}_q), \quad (38)$$

$$C_1 = \frac{1}{12}\sum_{pq} \sigma(\mathbf{e}_p, \mathbf{e}_q) - \frac{1}{20}\sum_{p} \sigma(\mathbf{e}_p, \mathbf{e}_p) - \frac{1}{10}\sum_{p<q} (\sigma(\mathbf{e}_{pq}^+, \mathbf{e}_{pq}^+) + \sigma(\mathbf{e}_{pq}^-, \mathbf{e}_{pq}^-)), \quad (39)$$

where p and q run over $\{x, y, z\}$ and $p < q$ over $\{xy, yz, xz\}$.

TABLE III. Value of the weight $\rho_l(b)$ of $\sigma(\mathbf{u}_l, \mathbf{v}_l^*)$ for the minimal 21 fourth-rank tensors $(\mathbf{u}_l, \mathbf{v}_l)$ to calculate S^{bb0} by Eq. (37) as well as C_0 and C_1 in Eq. (24). The basis unit vectors $\mathbf{e}_x$, $\mathbf{e}_y$, and $\mathbf{e}_z$ are along the three axes of $\mathbb{R}^3$, $\boldsymbol{\pi}^{\pm}_{mn} = (\pm i\mathbf{e}_m + \mathbf{e}_n)/\sqrt{2}$ and $\mathbf{e}^{\pm}_{mn} = (\pm\mathbf{e}_m + \mathbf{e}_n)/\sqrt{2}$.

l	$(\mathbf{u}_l, \mathbf{v}_l^*)$	$\rho_l(0)$	$\rho_l(1)$	$\rho_l(2)$	C_0	C_1
1	$(\mathbf{e}_x, \mathbf{e}_x)$	1/3	−1	−1/3	1/9	1/30
2	$(\mathbf{e}_x, \mathbf{e}_y)$	0	−1	0	1/9	1/12
3	$(\mathbf{e}_x, \mathbf{e}_z)$	0	−1	0	1/9	1/12
4	$(\mathbf{e}_y, \mathbf{e}_x)$	0	−1	0	1/9	1/12
5	$(\mathbf{e}_y, \mathbf{e}_y)$	1/3	−1	−1/3	1/9	1/30
6	$(\mathbf{e}_y, \mathbf{e}_z)$	0	−1	0	1/9	1/12
7	$(\mathbf{e}_z, \mathbf{e}_x)$	0	−1	0	1/9	1/12
8	$(\mathbf{e}_z, \mathbf{e}_y)$	0	−1	0	1/9	1/12
9	$(\mathbf{e}_z, \mathbf{e}_z)$	1/3	−1	−1/3	1/9	1/30
10	$(\boldsymbol{\pi}^+_{yz}, \boldsymbol{\pi}^-_{yz})$	−1/3	1/2	5/6	0	0
11	$(\boldsymbol{\pi}^-_{yz}, \boldsymbol{\pi}^+_{yz})$	−1/3	1/2	5/6	0	0
12	$(\boldsymbol{\pi}^+_{xz}, \boldsymbol{\pi}^-_{xz})$	−1/3	1/2	5/6	0	0
13	$(\boldsymbol{\pi}^-_{xz}, \boldsymbol{\pi}^+_{xz})$	−1/3	1/2	5/6	0	0
14	$(\boldsymbol{\pi}^+_{xy}, \boldsymbol{\pi}^-_{xy})$	−1/3	1/2	5/6	0	0
15	$(\boldsymbol{\pi}^-_{xy}, \boldsymbol{\pi}^+_{xy})$	−1/3	1/2	5/6	0	0
16	$(\mathbf{e}^+_{yz}, \mathbf{e}^+_{yz})$	1/3	1/2	1/6	0	−1/10
17	$(\mathbf{e}^-_{yz}, \mathbf{e}^-_{yz})$	1/3	1/2	1/6	0	−1/10
18	$(\mathbf{e}^+_{xz}, \mathbf{e}^+_{xz})$	1/3	1/2	1/6	0	−1/10
19	$(\mathbf{e}^-_{xz}, \mathbf{e}^-_{xz})$	1/3	1/2	1/6	0	−1/10
20	$(\mathbf{e}^+_{xy}, \mathbf{e}^+_{xy})$	1/3	1/2	1/6	0	−1/10
21	$(\mathbf{e}^-_{xy}, \mathbf{e}^-_{xy})$	1/3	1/2	1/6	0	−1/10

VI. RIXS FOR A POWDER WITH SYMMETRY

We can now combine the discussion of the influence of the symmetry of the sample and the number of $\phi(\epsilon_s, \epsilon)$ required to calculate the spectrum of a powdered material when the material itself has a symmetry.

The basic idea is quite simple. If G is the symmetry group of the material, we compute $\phi(\mathbf{u}_l, \mathbf{v}_l)$, where

$$\phi(\mathbf{u}_l, \mathbf{v}_l) = \sum_{imjn} u^*_{li} v^*_{lm} a_{im,jn} u_{lj} v_{ln},$$

for the 21 pairs of polarizations $(\mathbf{u}_l, \mathbf{v}_l)$ of Table III in terms of the n_G fundamental spectra of $a_{im,jn}$. This gives us a linear relation between $\phi(\mathbf{u}_l, \mathbf{v}_l)$ and the fundamental spectra described by a $n_G \times 21$ matrix whose null space represents the relations between different $\phi(\mathbf{u}_l, \mathbf{v}_l)$. For the example of a cubic material, the expression of $\phi(\mathbf{u}_l, \mathbf{v}_l)$ in terms of the four fundamental spectra $a_{11,11}$, $a_{11,22}$, $a_{12,12}$ and $a_{12,21}$ is

$$\begin{aligned}
\phi(\mathbf{e}_p, \mathbf{e}_q) &= a_{12,12} + \delta_{pq}(a_{11,11} - a_{12,12}),\\
\phi(\boldsymbol{\pi}^{\pm}_{pq}, \boldsymbol{\pi}^{\pm}_{pq}) &= \tfrac{1}{2}(a_{11,11} - a_{11,22} + a_{12,12} + a_{12,21}),\\
\phi(\mathbf{e}^{\pm}_{pq}, \mathbf{e}^{\pm}_{pq}) &= \tfrac{1}{2}(a_{11,11} + a_{11,22} + a_{12,12} + a_{12,21}),
\end{aligned}$$

for p and q equal to x, y, and z. The relations between $\phi(\mathbf{u}_l, \mathbf{v}_l)$ is then $\phi(\mathbf{e}_p, \mathbf{e}_p) = \phi(\mathbf{e}_x, \mathbf{e}_x)$ for all p, and for all $q \neq p$: $\phi(\mathbf{e}_p, \mathbf{e}_q) = \phi(\mathbf{e}_x, \mathbf{e}_y)$, $\phi(\boldsymbol{\pi}^{\pm}_{pq}, \boldsymbol{\pi}^{\pm}_{pq}) = \phi(\boldsymbol{\pi}^{\pm}_{xy}, \boldsymbol{\pi}^{\pm}_{xy})$ and $\phi(\mathbf{e}^{\pm}_{pq}, \mathbf{e}^{\pm}_{pq}) = \phi(\mathbf{e}^{\pm}_{xy}, \mathbf{e}^{\pm}_{xy})$. For a powder of a cubic sample, only four calculations are required to compute the full angular dependence of RIXS. This number reduces to three when the polarization state of the scattered beam is not measured, because $\phi(\boldsymbol{\pi}^{\pm}_{pq}, \boldsymbol{\pi}^{\pm}_{pq})$ is not needed.

We list now the fundamental spectra required to calculate the RIXS spectum of a powder of a sample with various symmetry groups. For all crystallographic point groups, the minimal number of spectra n_S and n_C needed to compute S_b and (C_0, C_1), respectively, is given in Table I.

A. For O, T_d, and O_h symmetry groups

In the previous paragraph, we showed that $\phi(\mathbf{u}_l, \mathbf{u}_v)$ can take only four different values. Thus, Eq. (37) becomes

$$\begin{aligned}
S_0 &= \sigma(\mathbf{e}_x, \mathbf{e}_x) + 2\sigma(\mathbf{e}^+_{xy}, \mathbf{e}^+_{xy}) - 2\sigma(\boldsymbol{\pi}^+_{xy}, \boldsymbol{\pi}^-_{xy}),\\
S_1 &= -3\sigma(\mathbf{e}_x, \mathbf{e}_x) - 6\sigma(\mathbf{e}_x, \mathbf{e}_y)\\
&\quad + 3\sigma(\mathbf{e}^+_{xy}, \mathbf{e}^+_{xy}) + 3\sigma(\boldsymbol{\pi}^+_{xy}, \boldsymbol{\pi}^-_{xy}),\\
S_2 &= -\sigma(\mathbf{e}_x, \mathbf{e}_x) + \sigma(\mathbf{e}^+_{xy}, \mathbf{e}^+_{xy}) + 5\sigma(\boldsymbol{\pi}^+_{xy}, \boldsymbol{\pi}^-_{xy}).
\end{aligned}$$

For polarization vectors normalized to unity and when the polarization of the scattered beam is not measured, three calculations are enough,

$$\begin{aligned}
C_0 &= \frac{\sigma(\mathbf{e}_x, \mathbf{e}_x) + 2\sigma(\mathbf{e}_x, \mathbf{e}_y)}{3},\\
C_1 &= \frac{\sigma(\mathbf{e}_x, \mathbf{e}_x) + 5\sigma(\mathbf{e}_x, \mathbf{e}_y) - 6\sigma(\mathbf{e}^+_{xy}, \mathbf{e}^+_{xy})}{10}.
\end{aligned}$$

B. For T or T_h

For the groups T and T_h, the relations between $\phi(\mathbf{u}_l, \mathbf{v}_l)$ are

$$\begin{aligned}
&\phi(\mathbf{e}^-_{yz}, \mathbf{e}^-_{yz}) = \phi(\mathbf{e}^+_{yz}, \mathbf{e}^+_{yz}) = \phi(\mathbf{e}^-_{xz}, \mathbf{e}^-_{xz}) = \phi(\mathbf{e}^+_{xz}, \mathbf{e}^+_{xz})\\
&\qquad = \phi(\mathbf{e}^-_{xy}, \mathbf{e}^-_{xy}) = \phi(\mathbf{e}^+_{xy}, \mathbf{e}^+_{xy}),\\
&\phi(\boldsymbol{\pi}^-_{yz}, \boldsymbol{\pi}^-_{yz}) = \phi(\boldsymbol{\pi}^+_{yz}, \boldsymbol{\pi}^+_{yz}) = \phi(\boldsymbol{\pi}^-_{xz}, \boldsymbol{\pi}^-_{xz}) = \phi(\boldsymbol{\pi}^+_{xz}, \boldsymbol{\pi}^+_{xz})\\
&\qquad = \phi(\boldsymbol{\pi}^-_{xy}, \boldsymbol{\pi}^-_{xy}) = \phi(\boldsymbol{\pi}^+_{xy}, \boldsymbol{\pi}^+_{xy}),\\
&\phi(\mathbf{e}_x, \mathbf{e}_x) = \phi(\mathbf{e}_y, \mathbf{e}_y) = \phi(\mathbf{e}_z, \mathbf{e}_z),\\
&\phi(\mathbf{e}_x, \mathbf{e}_y) = \phi(\mathbf{e}_y, \mathbf{e}_z) = \phi(\mathbf{e}_z, \mathbf{e}_x),\\
&\phi(\mathbf{e}_y, \mathbf{e}_x) = \phi(\mathbf{e}_z, \mathbf{e}_y) = \phi(\mathbf{e}_x, \mathbf{e}_z).
\end{aligned}$$

We need five calculations for the full spectrum

$$\begin{aligned}
S_0 &= \sigma(\mathbf{e}_x, \mathbf{e}_x) + 2\sigma(\mathbf{e}^+_{xy}, \mathbf{e}^+_{xy}) - 2\sigma(\boldsymbol{\pi}^+_{xy}, \boldsymbol{\pi}^-_{xy}),\\
S_1 &= -3\sigma(\mathbf{e}_x, \mathbf{e}_x) - 3\sigma(\mathbf{e}_x, \mathbf{e}_y) - 3\sigma(\mathbf{e}_y, \mathbf{e}_x)\\
&\quad + 3\sigma(\mathbf{e}^+_{xy}, \mathbf{e}^+_{xy}) + 3\sigma(\boldsymbol{\pi}^+_{xy}, \boldsymbol{\pi}^-_{xy}),\\
S_2 &= -\sigma(\mathbf{e}_x, \mathbf{e}_x) + \sigma(\mathbf{e}^+_{xy}, \mathbf{e}^+_{xy}) + 5\sigma(\boldsymbol{\pi}^+_{xy}, \boldsymbol{\pi}^-_{xy}).
\end{aligned}$$

And we need four calculations if the polarization state of the scattered beam is not measured,

$$\begin{aligned}
C_0 &= \frac{\sigma(\mathbf{e}_x, \mathbf{e}_x) + \sigma(\mathbf{e}_x, \mathbf{e}_y) + \sigma(\mathbf{e}_y, \mathbf{e}_x)}{3},\\
C_1 &= \frac{\sigma(\mathbf{e}_x, \mathbf{e}_x)}{10} + \frac{\sigma(\mathbf{e}_x, \mathbf{e}_y) + \sigma(\mathbf{e}_y, \mathbf{e}_x)}{4} - \frac{3\sigma(\mathbf{e}^+_{xy}, \mathbf{e}^+_{xy})}{5}.
\end{aligned}$$

C. For D_3, D_{3d}, C_{3v}, D_6, C_{6v}, D_{3h}, and D_{6h}

For the groups D_3, D_{3d}, or C_{3v}, the relations between $\phi(\mathbf{u}_l, \mathbf{v}_l)$ are not the same as those for D_6, C_{6v}, D_{3h}, or D_{6h},

but the differences compensate each other and the same final formulas for S_b are obtained. Indeed, the relations between $\phi(\mathbf{u}_l, \mathbf{v}_l)$ for D_3 are

$$\begin{aligned}
\phi(\mathbf{e}^+_{xz}, \mathbf{e}^+_{xz}) &= \tfrac{1}{2}(\phi(\mathbf{e}^-_{yz}, \mathbf{e}^-_{yz}) + \phi(\mathbf{e}^+_{yz}, \mathbf{e}^+_{yz})),\\
\phi(\mathbf{e}^-_{xz}, \mathbf{e}^-_{xz}) &= \phi(\mathbf{e}^+_{xz}, \mathbf{e}^+_{xz}),\\
\phi(\mathbf{e}^-_{xy}, \mathbf{e}^-_{xy}) &= \phi(\mathbf{e}^+_{xy}, \mathbf{e}^+_{xy}) = \phi(\mathbf{e}_y, \mathbf{e}_y) = \phi(\mathbf{e}_x, \mathbf{e}_x),\\
\phi(\boldsymbol{\pi}^+_{xz}, \boldsymbol{\pi}^+_{xz}) &= \tfrac{1}{2}(\phi(\boldsymbol{\pi}^-_{yz}, \boldsymbol{\pi}^-_{yz}) + \phi(\boldsymbol{\pi}^+_{yz}, \boldsymbol{\pi}^+_{yz})),\\
\phi(\boldsymbol{\pi}^-_{xz}, \boldsymbol{\pi}^-_{xz}) &= \phi(\boldsymbol{\pi}^+_{xz}, \boldsymbol{\pi}^+_{xz}),\\
\phi(\boldsymbol{\pi}^-_{xy}, \boldsymbol{\pi}^-_{xy}) &= \phi(\boldsymbol{\pi}^+_{xy}, \boldsymbol{\pi}^+_{xy}),\\
\phi(\mathbf{e}_z, \mathbf{e}_y) &= \phi(\mathbf{e}_z, \mathbf{e}_x),\\
\phi(\mathbf{e}_y, \mathbf{e}_z) &= \phi(\mathbf{e}_x, \mathbf{e}_z),\\
\phi(\mathbf{e}_y, \mathbf{e}_x) &= \phi(\mathbf{e}_x, \mathbf{e}_y),
\end{aligned}$$

while for D_6 they are

$$\begin{aligned}
\phi(\mathbf{e}^-_{yz}, \mathbf{e}^-_{yz}) &= \phi(\mathbf{e}^+_{yz}, \mathbf{e}^+_{yz}) = \phi(\mathbf{e}^-_{xz}, \mathbf{e}^-_{xz}) = \phi(\mathbf{e}^+_{xz}, \mathbf{e}^+_{xz}),\\
\phi(\boldsymbol{\pi}^-_{yz}, \boldsymbol{\pi}^-_{yz}) &= \phi(\boldsymbol{\pi}^+_{yz}, \boldsymbol{\pi}^+_{yz}) = \phi(\boldsymbol{\pi}^-_{xz}, \boldsymbol{\pi}^-_{xz}) = \phi(\boldsymbol{\pi}^+_{xz}, \boldsymbol{\pi}^+_{xz}),\\
\phi(\mathbf{e}^-_{xy}, \mathbf{e}^-_{xy}) &= \phi(\mathbf{e}^+_{xy}, \mathbf{e}^+_{xy}) = \phi(\mathbf{e}_y, \mathbf{e}_y) = \phi(\mathbf{e}_x, \mathbf{e}_x),\\
\phi(\boldsymbol{\pi}^-_{xy}, \boldsymbol{\pi}^-_{xy}) &= \phi(\boldsymbol{\pi}^+_{xy}, \boldsymbol{\pi}^+_{xy}),\\
\phi(\mathbf{e}_z, \mathbf{e}_y) &= \phi(\mathbf{e}_z, \mathbf{e}_x),\\
\phi(\mathbf{e}_y, \mathbf{e}_z) &= \phi(\mathbf{e}_x, \mathbf{e}_z),\\
\phi(\mathbf{e}_y, \mathbf{e}_x) &= \phi(\mathbf{e}_x, \mathbf{e}_y).
\end{aligned}$$

When the polarization state of the scattered beam is not measured we need six calculations,

$$\begin{aligned}
C_0 &= \frac{2}{9}(\sigma(\mathbf{e}_x, \mathbf{e}_x) + \sigma(\mathbf{e}_x, \mathbf{e}_y) + \sigma(\mathbf{e}_x, \mathbf{e}_z) + \sigma(\mathbf{e}_z, \mathbf{e}_x))\\
&\quad + \frac{\sigma(\mathbf{e}_z, \mathbf{e}_z)}{9},\\
C_1 &= -\frac{2}{15}\sigma(\mathbf{e}_x, \mathbf{e}_x) + \frac{\sigma(\mathbf{e}_x, \mathbf{e}_y) + \sigma(\mathbf{e}_x, \mathbf{e}_z) + \sigma(\mathbf{e}_z, \mathbf{e}_x)}{6}\\
&\quad + \frac{\sigma(\mathbf{e}_z, \mathbf{e}_z)}{30} - \frac{2}{5}\sigma(\mathbf{e}^+_{xz}, \mathbf{e}^+_{xz}).
\end{aligned}$$

For the full spectra, we need eight calculations,

$$\begin{aligned}
S_0 &= \tfrac{4}{3}\sigma(\mathbf{e}_x, \mathbf{e}_x) + \tfrac{1}{3}\sigma(\mathbf{e}_z, \mathbf{e}_z) - \tfrac{2}{3}\sigma(\boldsymbol{\pi}^+_{xy}, \boldsymbol{\pi}^-_{xy})\\
&\quad - \tfrac{4}{3}\sigma(\boldsymbol{\pi}^+_{xz}, \boldsymbol{\pi}^-_{xz}) + \tfrac{4}{3}\sigma(\mathbf{e}^+_{xz}, \mathbf{e}^+_{xz}),\\
S_1 &= -\sigma(\mathbf{e}_x, \mathbf{e}_x) - 2\sigma(\mathbf{e}_x, \mathbf{e}_y) - 2\sigma(\mathbf{e}_x, \mathbf{e}_z)\\
&\quad - 2\sigma(\mathbf{e}_z, \mathbf{e}_x) - \sigma(\mathbf{e}_z, \mathbf{e}_z) + \sigma(\boldsymbol{\pi}^+_{xy}, \boldsymbol{\pi}^-_{xy})\\
&\quad + 2\sigma(\boldsymbol{\pi}^+_{xz}, \boldsymbol{\pi}^-_{xz}) + 2\sigma(\mathbf{e}^+_{xz}, \mathbf{e}^+_{xz}),\\
S_2 &= -\tfrac{1}{3}\sigma(\mathbf{e}_x, \mathbf{e}_x) - \tfrac{1}{3}\sigma(\mathbf{e}_z, \mathbf{e}_z) + \tfrac{5}{3}\sigma(\boldsymbol{\pi}^+_{xy}, \boldsymbol{\pi}^-_{xy})\\
&\quad + \tfrac{10}{3}\sigma(\boldsymbol{\pi}^+_{xz}, \boldsymbol{\pi}^-_{xz}) + \tfrac{2}{3}\sigma(\mathbf{e}^+_{xz}, \mathbf{e}^+_{xz}).
\end{aligned}$$

D. For C_6, C_{3h}, and C_{6h}

For the groups C_6, C_{3h}, and C_{6h}, when the polarization of the scattered beam is not measured, C_0 and C_1 are the same as for D_3 in Sec. VI C and, when it is measured, the values of S_b are obtained by replacing $\sigma(\boldsymbol{\pi}^+_{xy}, \boldsymbol{\pi}^-_{xy})$ with $\sigma(\boldsymbol{\pi}^+_{xy}, \boldsymbol{\pi}^-_{xy})/2 + \sigma(\boldsymbol{\pi}^-_{xy}, \boldsymbol{\pi}^+_{xy})/2$ in the expressions for S_b given in Sec. VI C.

E. For D_4, C_{4v}, D_{2d}, and D_{4h}

For the groups D_4 or C_{4v} or D_{2d}, or D_{4h} the relations between $\phi(\mathbf{u}_l, \mathbf{v}_l)$ are

$$\begin{aligned}
\phi(\mathbf{e}^-_{yz}, \mathbf{e}^-_{yz}) &= \phi(\mathbf{e}^+_{yz}, \mathbf{e}^+_{yz}) = \phi(\mathbf{e}^-_{xz}, \mathbf{e}^-_{xz}) = \phi(\mathbf{e}^+_{xz}, \mathbf{e}^+_{xz}),\\
\phi(\boldsymbol{\pi}^-_{yz}, \boldsymbol{\pi}^-_{yz}) &= \phi(\boldsymbol{\pi}^+_{yz}, \boldsymbol{\pi}^+_{yz}) = \phi(\boldsymbol{\pi}^-_{xz}, \boldsymbol{\pi}^-_{xz}) = \phi(\boldsymbol{\pi}^+_{xz}, \boldsymbol{\pi}^+_{xz}),\\
\phi(\mathbf{e}^-_{xy}, \mathbf{e}^-_{xy}) &= \phi(\mathbf{e}^+_{xy}, \mathbf{e}^+_{xy}),\\
\phi(\boldsymbol{\pi}^-_{xy}, \boldsymbol{\pi}^-_{xy}) &= \phi(\boldsymbol{\pi}^+_{xy}, \boldsymbol{\pi}^+_{xy}),\\
\phi(\mathbf{e}_x, \mathbf{e}_x) &= \phi(\mathbf{e}_y, \mathbf{e}_y),\\
\phi(\mathbf{e}_z, \mathbf{e}_y) &= \phi(\mathbf{e}_z, \mathbf{e}_x),\\
\phi(\mathbf{e}_y, \mathbf{e}_z) &= \phi(\mathbf{e}_x, \mathbf{e}_z),\\
\phi(\mathbf{e}_y, \mathbf{e}_x) &= \phi(\mathbf{e}_x, \mathbf{e}_y).
\end{aligned}$$

When the polarization state of the scattered beam is not measured we need seven calculations,

$$\begin{aligned}
C_0 &= \frac{2}{9}(\sigma(\mathbf{e}_x, \mathbf{e}_x) + \sigma(\mathbf{e}_x, \mathbf{e}_y) + \sigma(\mathbf{e}_x, \mathbf{e}_z) + \sigma(\mathbf{e}_z, \mathbf{e}_x))\\
&\quad + \frac{\sigma(\mathbf{e}_z, \mathbf{e}_z)}{9},\\
C_1 &= \frac{1}{15}\sigma(\mathbf{e}_x, \mathbf{e}_x) + \frac{\sigma(\mathbf{e}_x, \mathbf{e}_y) + \sigma(\mathbf{e}_x, \mathbf{e}_z) + \sigma(\mathbf{e}_z, \mathbf{e}_x)}{6}\\
&\quad + \frac{\sigma(\mathbf{e}_z, \mathbf{e}_z)}{30} - \frac{1}{5}\sigma(\mathbf{e}^+_{xy}, \mathbf{e}^+_{xy}) - \frac{2}{5}\sigma(\mathbf{e}^+_{xz}, \mathbf{e}^+_{xz}).
\end{aligned}$$

For the full spectra we need nine calculations,

$$\begin{aligned}
S_0 &= \tfrac{2}{3}\sigma(\mathbf{e}_x, \mathbf{e}_x) + \tfrac{1}{3}\sigma(\mathbf{e}_z, \mathbf{e}_z) - \tfrac{2}{3}\sigma(\boldsymbol{\pi}^+_{xy}, \boldsymbol{\pi}^-_{xy})\\
&\quad - \tfrac{4}{3}\sigma(\boldsymbol{\pi}^+_{xz}, \boldsymbol{\pi}^-_{xz}) + \tfrac{2}{3}\sigma(\mathbf{e}^+_{xy}, \mathbf{e}^+_{xy}) + \tfrac{4}{3}\sigma(\mathbf{e}^+_{xz}, \mathbf{e}^+_{xz}),\\
S_1 &= -2\sigma(\mathbf{e}_x, \mathbf{e}_x) - 2\sigma(\mathbf{e}_x, \mathbf{e}_y) - 2\sigma(\mathbf{e}_x, \mathbf{e}_z)\\
&\quad - 2\sigma(\mathbf{e}_z, \mathbf{e}_x) - \sigma(\mathbf{e}_z, \mathbf{e}_z) + \sigma(\boldsymbol{\pi}^+_{xy}, \boldsymbol{\pi}^-_{xy})\\
&\quad + 2\sigma(\boldsymbol{\pi}^+_{xz}, \boldsymbol{\pi}^-_{xz}) + \sigma(\mathbf{e}^+_{xy}, \mathbf{e}^+_{xy}) + 2\sigma(\mathbf{e}^+_{xz}, \mathbf{e}^+_{xz}),\\
S_2 &= -\tfrac{2}{3}\sigma(\mathbf{e}_x, \mathbf{e}_x) - \tfrac{1}{3}\sigma(\mathbf{e}_z, \mathbf{e}_z) + \tfrac{5}{3}\sigma(\boldsymbol{\pi}^+_{xy}, \boldsymbol{\pi}^-_{xy})\\
&\quad + \tfrac{10}{3}\sigma(\boldsymbol{\pi}^+_{xz}, \boldsymbol{\pi}^-_{xz}) + \tfrac{1}{3}\sigma(\mathbf{e}^+_{xy}, \mathbf{e}^+_{xy}) + \tfrac{2}{3}\sigma(\mathbf{e}^+_{xz}, \mathbf{e}^+_{xz}).
\end{aligned}$$

F. For C_4, S_4, and C_{4h}

For the groups C_4, S_4 and C_{4h}, when the polarization of the scattered beam is not measured, C_0 and C_1 are the same as for D_4 in Sec. VI E and, when it is measured, the values of S_b are obtained by replacing $\sigma(\boldsymbol{\pi}^+_{xy}, \boldsymbol{\pi}^-_{xy})$ with $\sigma(\boldsymbol{\pi}^+_{xy}, \boldsymbol{\pi}^-_{xy})/2 + \sigma(\boldsymbol{\pi}^-_{xy}, \boldsymbol{\pi}^+_{xy})/2$ in the expressions for S_b given in Sec. VI E.

VII. APPLICATIONS

A. General experiment considerations

In a RIXS experiment, depending on the energy range of the scattered photon, detection is achieved using an emission spectrometer that can either utilize grazing incidence diffraction gratings for soft x-rays or crystal analyzers for hard

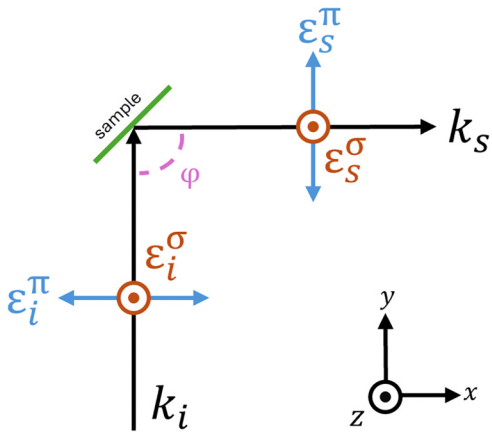

FIG. 1. Schematic showing an overview of experiment configuration. Parallel and perpendicular polarization vectors are denoted as π and σ, respectively. The incident and scattered photon momentum are denoted as $\widehat{\mathbf{k}}_i$ and $\widehat{\mathbf{k}}_s$, respectively. The angle of scattered photon detection is given by φ.

x-rays. The sample, crystal analyzer, and detector sit within a Rowland circle.

With reference to Fig. 1, the incoming incident beam is denoted by $\widehat{\mathbf{k}}_i$ and the emitted fluorescence photons ($\widehat{\mathbf{k}}_s$) that are scattered by the sample are energy discriminated using crystal analyzers, before detection, at an angle φ with respect to $\widehat{\mathbf{k}}_i$. The crystal analyzer is usually positioned at 90°, with respect to the incoming incident beam ($\widehat{\mathbf{k}}_i$), and serves as the reference point from which additional crystal analyzers can be positioned either side.

The derivations for powder samples from the present paper lead to several general experimental conclusions:

(i) The RIXS cross section measured with incident vertical polarization and standard $\varphi = 90^\circ$ horizontal scattering geometry is identical to the RIXS cross-section measured with incident horizontal polarization and back-scattering horizontal geometry.

(ii) In hard x-ray RIXS, the use of multiple crystal analyzers leads to the summation of different RIXS spectra unless each of their intensity is detected individually using a 2D detector.

(iii) Theoretical modeling should then be performed accordingly using the provided formulas. For cubic samples, four spectra need to be computed to obtain the correct RIXS cross section of a powder, contrary to standard XAS where only one spectrum is needed.

B. Example of application: Ni^{II} $2p3d$ RIXS

Ni^{II} in an octahedral crystal field is the archetypal example to illustrate how to apply the formulae provided in the present paper, which would correlate to the case of NiO [48]. A crystal field, $10Dq$, value of 1 eV was used as a typical value for Ni^{II} in oxides [48–50]. The Slater integrals were reduced by 80% from the Hartree-Fock values and spin-orbit coupling is fully considered. More information can be found in Appendix. In order to calculate the $2p3d$ RIXS of a powder sample, we use Eq. (23) and Sec. VI A and thus calculate the four fundamental spectra: $\sigma(\mathbf{e}_x, \mathbf{e}_x)$, $\sigma(\mathbf{e}_x, \mathbf{e}_y)$, $\sigma(\mathbf{e}_{xy}^+, \mathbf{e}_{xy}^+)$, and $\sigma(\boldsymbol{\pi}_{xy}^+, \boldsymbol{\pi}_{xy}^-)$. Figure 2 shows these four RIXS maps around the Ni L_3-edge. If the polarization of the emitted x-rays is not measured, then we calculate the RIXS cross section defined in Eq. (24) using the expressions of C_0 and C_1 written in terms of the fundamental spectra (Sec. VI A). The C_0 and C_1 are represented in Fig. 3. C_0 is the RIXS spectrum that would be measured with a detector covering all directions in space.

Then, using Eq. (24), one can compute the RIXS spectra in different experimental conditions. For example, assuming horizontal incident linear polarization of the x-rays, Fig. 4(a) shows the $2p3d$ RIXS map for $\varphi = 90^\circ$ scattering angle ($\epsilon \parallel \mathbf{k}_s$) and Fig. 4(b) shows the $2p3d$ RIXS map for $\varphi = 0^\circ$($\epsilon \perp \mathbf{k}_s$). Figure 4(c) shows selected constant-incident-energy (CIE) cuts through the RIXS spectrum corresponding the maximum of the L_3 edge and additional satellite peaks, the residuals between both polarization cases are shown in Fig. 4(d). The difference agrees with previous observations [51]. From these results, we observe that the angular dependence of $2p3d$ RIXS of Ni^{II} in an octahedral crystal field is weak. We move on to actinides to explore stronger effects.

C. Case study: Actinide $3d4f$ RIXS

The formulas derived within Sec. VI have been applied to a selection of actinide compounds, previously published and measured using $3d4f$ RIXS. It is to be emphasized though, that the derivations are applicable to all RIXS measurements, regardless of which absorption and emission lines are probed.

With respect to actinide x-ray spectroscopy, $3d4f$ RIXS is a photon-in photon-out inelastic scattering process of which a $3d$ core electron is resonantly excited into the unoccupied valence $5f$ states, while simultaneously detecting fluorescence photons emitted from a $4f \rightarrow 3d$ decay. From herein, when discussing $3d4f$ RIXS simulations, these will correspond to the actinide M_4-edge absorption as a function of the N_6 (M_β) emission line. The complete $3d4f$ RIXS process is shown in Fig. 5.

Actinide $3d4f$ RIXS falls within the tender x-ray region. As such, performing these measurements does not require ultrahigh vacuum environments but are yet capable of providing high resolution spectra, exposing spectral features that are otherwise hidden by the large core-hole lifetime broadening if measuring hard x-ray spectroscopy or conventional XAS. This balance of experiment conditions and spectral resolution lends itself as a quintessential technique for probing actinides. Because of this reasoning, $3d4f$ RIXS is increasingly being utilized as the technique to probe the valence actinide $5f$ orbitals to investigate and gain insights into actinide electronic structure, local coordination, redox, and their subsequent role in covalency [52–64].

However, owing to the relative short divergence of φ from the reference crystal analyzers positioned at $\varphi = 90^\circ$, we show in Figs. 6–8 that $3d4f$ RIXS measurements performed using these emission spectrometer orientations miss the wealth of information that could otherwise be revealed if the crystal analyzers are positioned towards more extreme back-scattering geometries, ($\varphi : 90^\circ \rightarrow 0^\circ$).

To emphasize the contrast of additional information that can be extracted by $3d4f$ RIXS, a systematic selection of three uranium compounds, previously published and

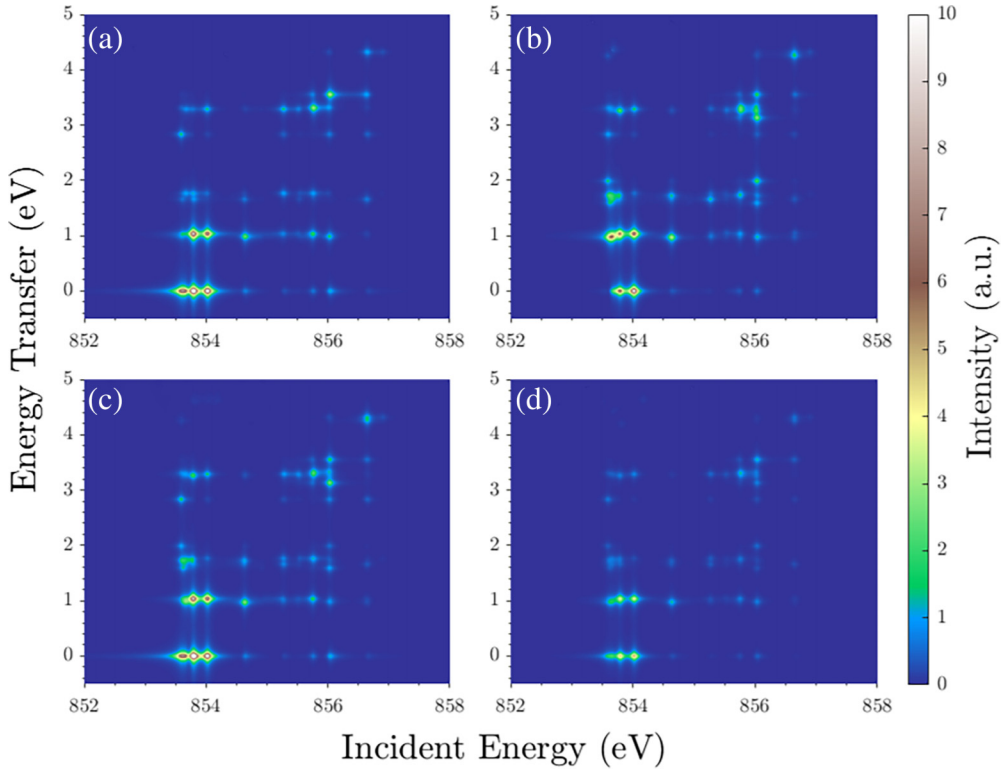

FIG. 2. Fundamental spectra of Ni^{II} $2p3d$ RIXS, around the L_3 absorption edge. (a) $\sigma(\mathbf{e}_x, \mathbf{e}_x)$, (b) $\sigma(\mathbf{e}_x, \mathbf{e}_y)$, (c) $\sigma(\mathbf{e}^+_{xy}, \mathbf{e}^+_{xy})$, and (d) $\sigma(\boldsymbol{\pi}^+_{xy}, \boldsymbol{\pi}^-_{xy})$.

measured, with common U oxidation states and varying local point-group symmetry have been chosen as case studies, namely, $U^{VI}O_2Cl_4^{2-}$ (D_{4h}) [55], $Sr_3U^{VI}O_6$ (O_h) [55], and $U^{IV}O_2$ (O_h) [65], where U^{VI} and U^{IV} have $5f^0$ and $5f^2$ ground-state electronic structures, respectively. We will consider as typical instrument a five-crystal analyzer spectrometer, as has been developed on several beamlines [66–70].

In Figs. 6(c) and 6(d), the simulated RIXS maps correspond to crystal analyzers positioned at $\varphi = 90°$ and $90° \pm 30°$; this is representative of most divergent positions of typical five-analyzers emission spectrometers, which typically have crystal analyzers at these positions and $\varphi = 90° \pm 15°$, which we do not account for. In order to further highlight the contrast in the possible spectra obtainable, Fig. 6(e) correlates

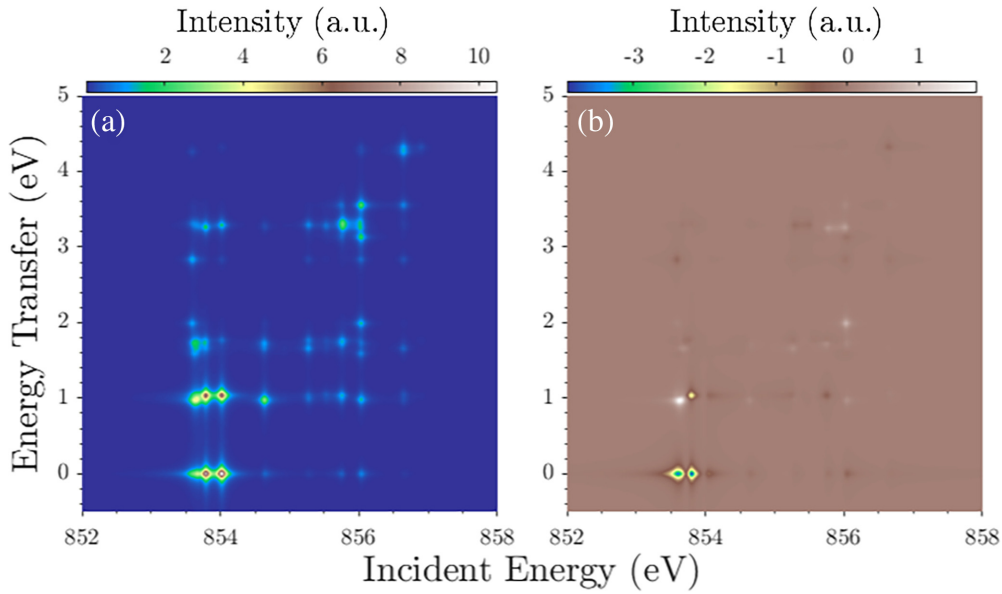

FIG. 3. (a) C_0 and (b) C_1 components of Ni^{II} $2p3d$ RIXS spectra as defined by Eq. (24).

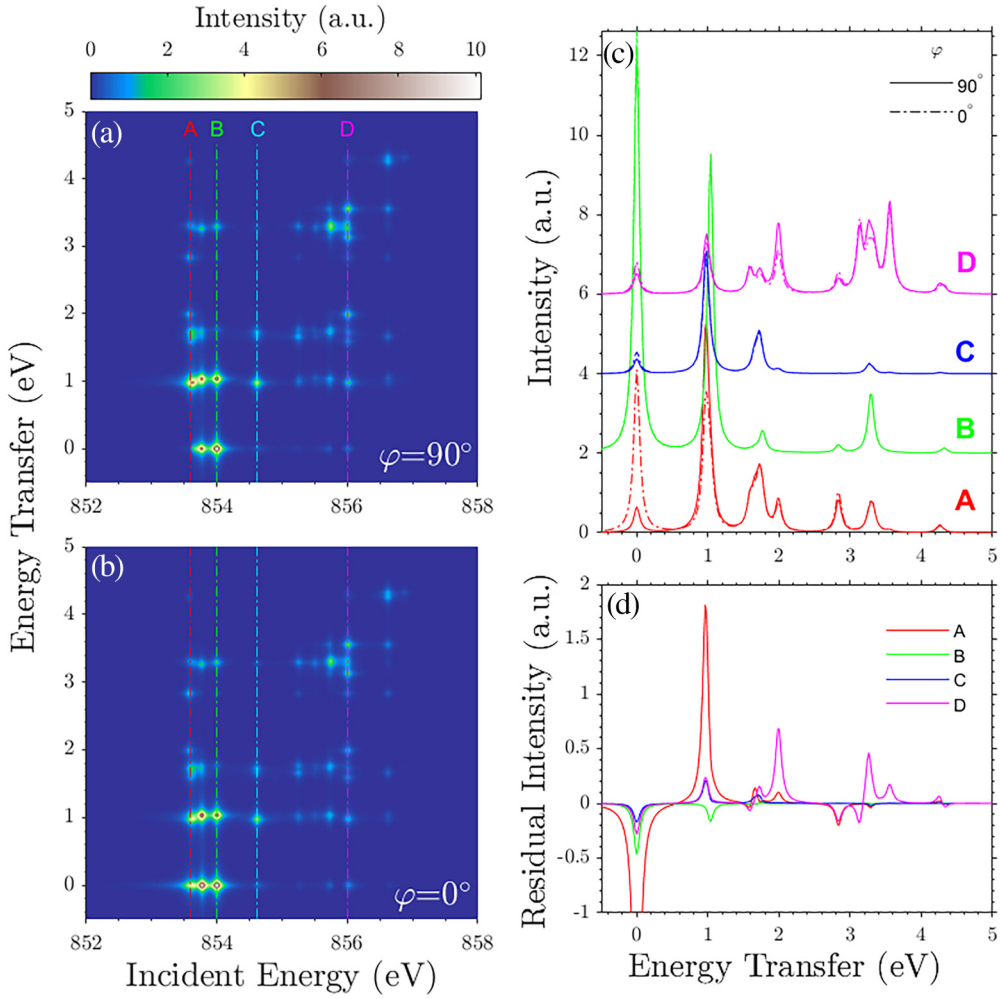

FIG. 4. Ni^{II} calculated $2p3d$ RIXS maps at (a) $\varphi = 90°$ and (b) $\varphi = 0°$ (backscattering). (c) Selected CIE cuts through RIXS maps (a) and (b), represented by colored vertical lines (dot-dash). (d) Residual intensity of CIE cuts comparing (a) and (b) intensity.

to $\varphi = 0°$ and reflects when an emission spectrometer would be orientated in a backscattering geometry.

From these simulated $3d4f$ RIXS maps, constant-emission-energy (CEE) cuts can be taken [Fig. 6(a)], which are representative of experimentally obtained HERFD-XAS spectra, and correspond to the diagonal red-dash cuts through the $3d4f$ RIXS maps at the maximum of the N_6 (M_β) emission line. Characteristic spectral features of the CEE cut, peaks **C-E, G**, are associated to the main whiteline transition and the large $5f$ D_{4h} ligand field splitting, carrying sensitivity to the incoming incident energy. It is observed that when φ is varied from $90° \rightarrow 0°$, the intensity of these peaks are seemingly not perturbed, with the exception to the whiteline, peak **C**, which readily decreases in intensity when approaching backscattering geometries.

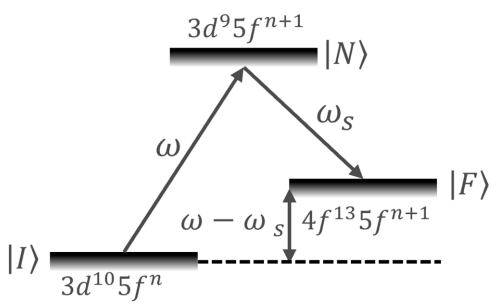

FIG. 5. Schematic of $3d4f$ RIXS, depicting the correlation between incident (ω), emitted (ω_s), and transferred (ω - ω_s) energies, and the corresponding electronic configurations of the initial $|I\rangle$, intermediate $|N\rangle$, and final $|F\rangle$ states.

Similarly, constant-incident-energy (CIE) cuts, Fig. 6(b), represented as vertical blue-dash cuts through the simulated $3d4f$ RIXS maps are representative of resonant x-ray emission spectroscopy (RXES) measurements, carrying sensitivity to the final state of the $3d4f$ RIXS process. As the example presented concerns U^{VI}, the remaining non-characterized intensity present in the simulated RIXS maps and prominently extracted in the CIE cuts, peaks **A-B, F, H**, arise from intershell $4f^{13}5f^1$ spin-exchange interactions, and commonly referred to as satellites. The intensity of these peaks increases drastically as a function of φ ($90\ °\rightarrow 0°$). It is also noted that the current most divergent crystal analyzer positions ($\varphi = 90° \pm 30°$) of typical five-analyzer spectrometer would be potentially adequate to capture partial intensity of these features in experiment

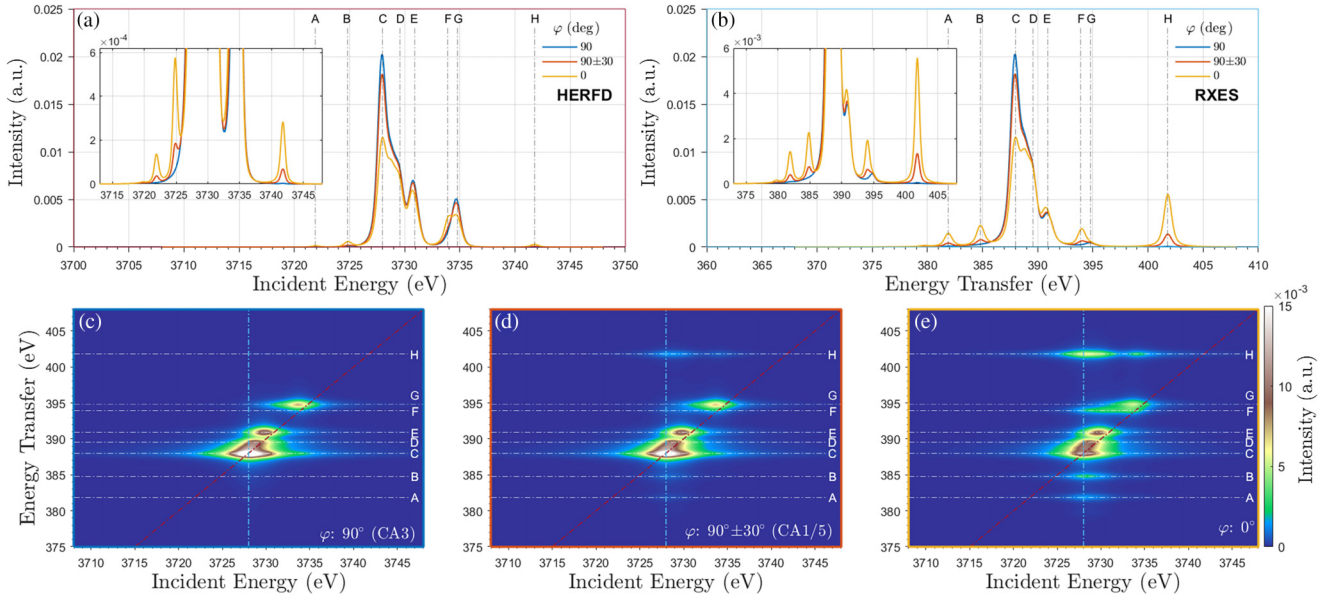

FIG. 6. $U^{VI}O_2Cl_4^{2-}$ (a) simulated HERFD cuts through $3d4f$ RIXS maps (c)–(e), inplot is same as (a) but with limited y axis. (b) Simulated RXES cuts through RIXS maps (c)–(e), inplot is same as (b) but with limited y axis. (c)–(e) simulated uranium M_4N_6 $3d4f$ RIXS maps at different crystal analyzer (CA) positions φ; 90°, 90° ± 30°, and backscattering case of 0°. HERFD (red dash) and RXES (blue dash) cuts are represented as the diagonal and vertical cuts in the maps. White horizontal lines [(c)–(e)] and black vertical lines [(a)(b)] correlate to the most prominent peaks present.

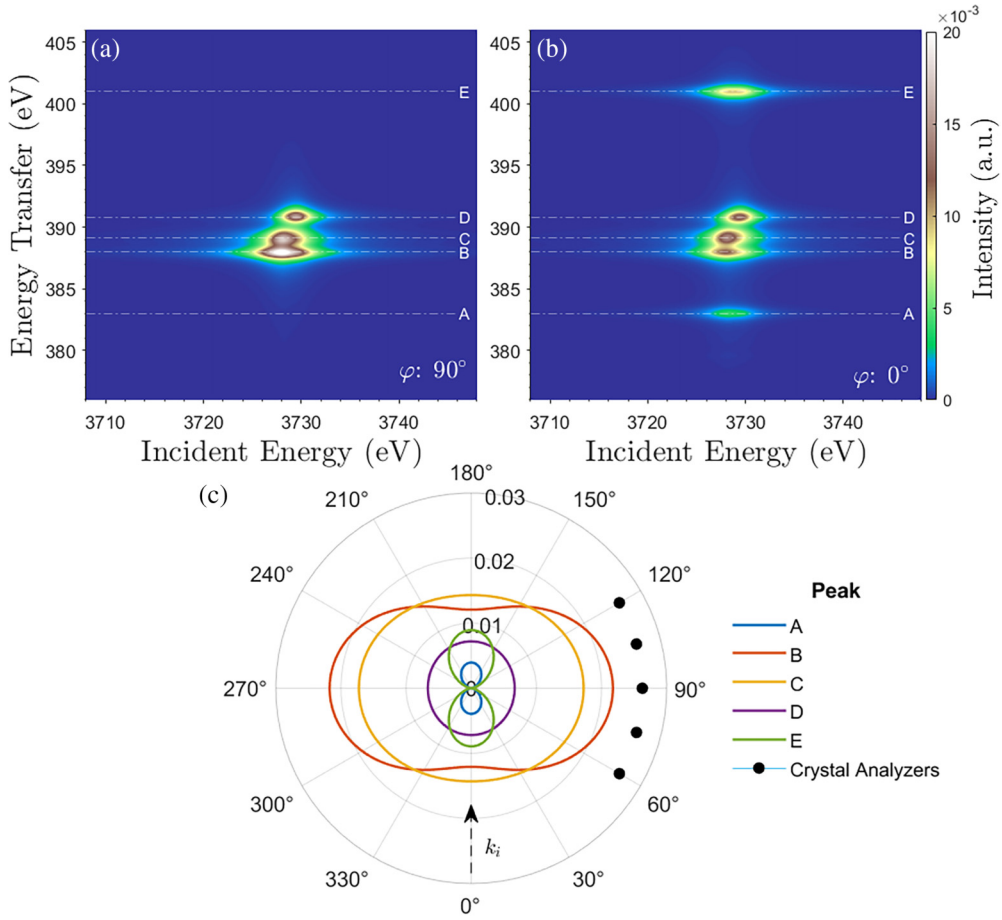

FIG. 7. $Sr_3U^{VI}O_6$ simulated uranium M_4N_6 $3d4f$ RIXS maps at (a) $\varphi = 90°$ and (b) $\varphi = 0°$ with respect to the incident beam, $\widehat{\mathbf{k}}_i$. (c) Polar plot of features **A**–**E**. The angular axis is representative of φ and the radial axis is the peak intensity. Example positions of crystal analyzers are indicated by black dots.

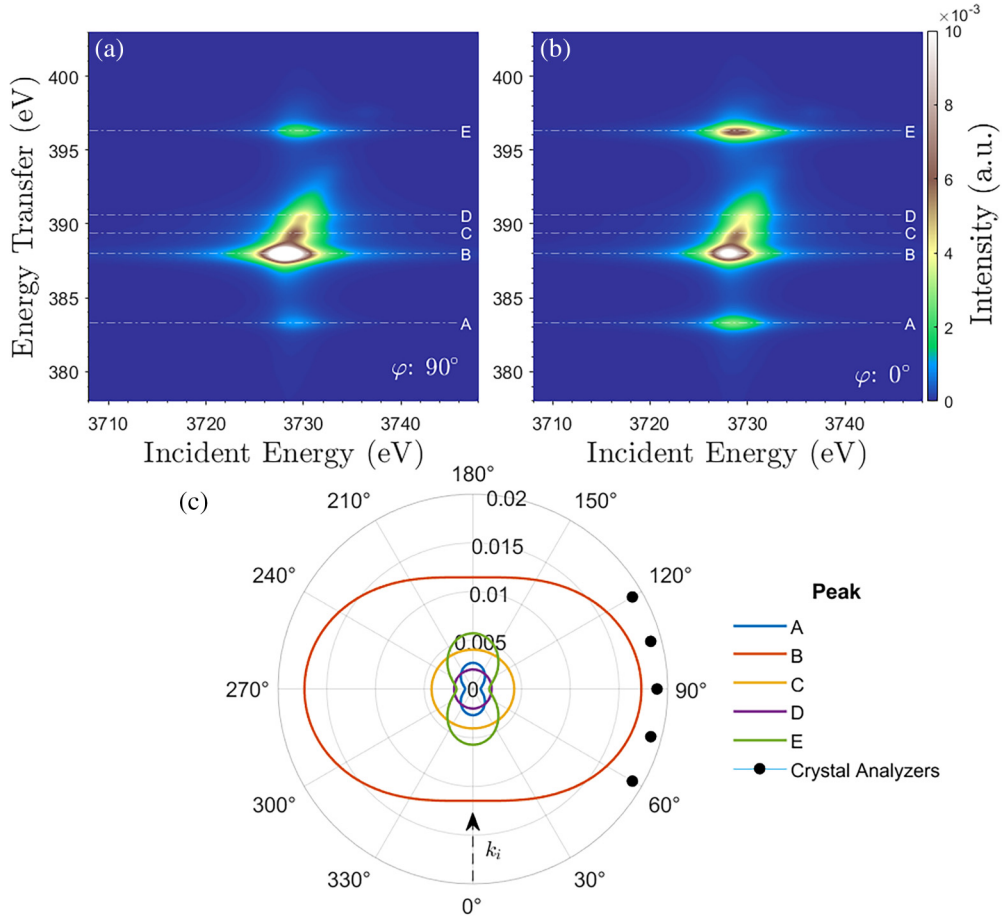

FIG. 8. $U^{IV}O_2$ simulated uranium M_4N_6 $3d4f$ RIXS maps at (a) $\varphi = 90°$ and (b) $\varphi = 0°$ with respect to the incident beam, $\widehat{\mathbf{k}}_i$. (c) Polar plot of features **A**–**E**. The angular axis is representative of φ and the radial axis is the peak intensity. Example positions of crystal analyzers are indicated by black dots.

conditions, depending on signal-noise and other experiment considerations.

Upon comparing simulations presented here using the derivations of Sec. VI with the simulations previously published [55], some key points are made. The authors previously modeled their experimental HERFD-XAS spectra of $U^{VI}O_2Cl_4^{2-}$ using an x-ray absorption ligand field multiplet model that considers the $5f$-ligand field splitting, $3d^95f^1$ repulsion and spin-exchange interactions, and spin-orbit coupling. Their best simulation of the $U^{VI}O_2Cl_4^{2-}$ HERFD data most noticeably required a scaling the $3d$-$5f$ Slater integrals to 50% of their atomic values. Conversely, what we present is that by employing a ligand field multiplet model that encompasses the entire $3d4f$ RIXS process, implying additional consideration in the simulations to include the $4f^{13}5f^1$ repulsion and spin-exchange interactions and their respective spin-orbit coupling constants, and that of which employs the equations for D_{4h} in Sec. VI, we are able to come close to reproducing the fine structure in their spectra. The key factor though is that in the simulations we present, the Slater integrals were solely scaled, conventionally, to 80% of their atomic value [71], with no other scaling required. Solely by accounting for the position of the crystal analyzers with respect to φ and the inclusion of our derivations when calculating the $3d4f$ RIXS spectra, we are, in general, able to now provide a method that more accurately simulates experimental data.

Maintaining a uranium $5f^0$ electronic configuration but changing the symmetry from $U^{VI}O_2Cl_4^{2-}$ D_{4h} to $Sr_3U^{VI}O_6$ O_h, the results are similar in nature. Figures 7(a) and 7(b) show simulated $3d4f$ RIXS maps of $Sr_3U^{VI}O_6$ in both extreme, perpendicular ($\varphi = 90°$) and backscattering ($\varphi = 0°$), geometries. It is clear that the experiment orientation has a limited sensitivity to peaks **B**–**D**, and can be attributed to the $5f$ ligand field splitting. Contrarily, peaks **A** and **E** carry significant sensitivity to the $4f$-$5f$ intershell spin-exchange interactions in the final state of $3d4f$ RIXS. Another perspective of analyzing the sensitivity of peak intensity, peaks **A**–**E**, as a function of φ is shown in Fig. 7(c). The intensity of the peaks is shown on the radial axis of the polar plot, while the angular axis shows φ, typical five-crystal analyzer φ positions are shown as a reference emission spectrometer configuration. When measuring perpendicular to the incident beam ($\varphi = 90°$), the intensity of peaks **A** and **E** approach 0 and would not be observed experimentally, whilst all other features are at their maxima. Conversely, at $\varphi = 0°$, this relation is inverted such that the satellite intensities are at their respective maxima and peaks **B**–**D** are at their lowest.

Maintaining O_h symmetry but diverging from U^{VI} $5f^0$ ($Sr_3U^{VI}O_6$) to U^{IV} $5f^2$ ($U^{IV}O_2$) ground-state electronic

configuration subsequently results in Fig. 8. Prior to characterizing the features present in the simulations, starting from a $5f^2$ ground-state electronic structure, this subsequently leads to an intermediate $|\mathrm{N}\rangle\ 3d^9 5f^3$ and final $|\mathrm{F}\rangle\ 4f^{13}5f^3$ state electronic configuration during the RIXS process. With particular emphasis to the final state electronic configuration, it consequently leads to necessity to consider $4f$-$5f$ and $5f$-$5f$ intershell spin-exchange and repulsion interactions. Comparing Figs. 7(c) and 8(c), where the experiment geometry is perpendicular to the incoming beam ($\varphi = 90^\circ$), peaks **A** and **E** would each now have observable intensity in $\mathrm{U^{IV}}$ experimental $3d4f$ RIXS measurements. The same observations as before, with reference to Fig. 8(c), are observed when the crystal analyzers are orientated perpendicular to the incoming beam ($\varphi = 90^\circ$), the main whiteline intensity and features **B**–**D** arising from the $5f$-ligand field splitting are most intense. Additionally secluded within these peaks, however, is intensity that originates from $5f$-$5f$ repulsion interactions, although it is proposed that φ carries minor influence on the intensity of these features. Although, when approaching backscattering geometry ($\varphi = 90^\circ \rightarrow 0^\circ$), the satellites corresponding to intershell $4f$-$5f$ spin-exchange interaction are most prominent, following the same trends as $\mathrm{U^{VI}}$.

As previous authors have used the energy position and intensities of the satellites to gain information into the effective value of Slater integrals to further derive insights into chemical bonding, we show, however, that the implication from these examples, such satellites present in $3d4f$ RIXS, and others, can serve as an anchor for determining the correct scaling of Slater integrals, as solely the intensity of these features are perturbed as function of φ, not their energetic positioning, which only changes as a consequence of scaling.

To further elaborate on the sensitivity of $3d4f$ RIXS to intershell $5f$-$5f$ repulsion and $4f$-$5f$ spin-exchange interactions, a series of $\mathrm{An^{IV}O_2}$ (An = Th, Np, Pu) in cubic symmetry (O_h) as previously published [65] have been simulated as example cases where the ground state $5f$ electron occupancy changes from $5f^0$ to $5f^3$ to $5f^4$ respectively. Additionally, an example of angular dependency for uranium $\mathrm{M_5N_{6,7}}$ ($\mathrm{M_5M\alpha_{1,2}}$) $3d4f$ RIXS is presented for $\mathrm{U^{IV}O_2}$. These can be found in the Supplemental Material [27].

VIII. CONCLUSIONS AND PROSPECTS

In this work, we provide a general method—applicable to all point-group symmetries—to express a RIXS spectrum in terms of its fundamental spectra. In other words, we determined the minimal number of spectra that must be measured or calculated in order to fully access all the spectral information contained in a sample. The analysis was carried out within the electric-dipole approximation for both the incoming and outgoing photons.

A direct application of this approach is the derivation of simple and practical expressions for the RIXS spectrum of isotropic samples with the most common sample symmetries (cubic, tetrahedral, hexagonal, trigonal, and tetragonal). We expect that these easy-to-use formulas will stimulate experimental measurements, in particular by exploring the dependence on the scattering angle and the polarization of the outgoing beam, which, for example, could help to enhance elusive spectral features by choosing more appropriate experimental configurations. Accounting for this dependence may also lead to a reexamination, and possibly a reinterpretation, of existing data in the literature.

To illustrate the derivations, we first take the example of the typical $\mathrm{Ni^{II}}$ $2p3d$ RIXS. Then, we show that there is a significant angular dependence in actinide $3d4f$ RIXS by simulating previously reported literature data. In each of these examples, we show that final-state RIXS satellite intensities are significantly perturbed as a function of the spectrometer geometry. As actinide x-ray measurements are performed on isotropic powder samples, we show that it is crucial to use the formulas presented in the present paper to correctly simulate satellite intensities and subsequently obtain the correct effective scaling for Slater integrals. Furthermore, from an experimental perspective, we highlight that ideal experiment conditions should use a 2D detector for RIXS measurements. This would facilitate spectrometer designs with a large divergence with respect to $\widehat{\mathbf{k}}_s$, and allow for the individual analysis of the scattered photon intensity from each crystal analyzer.

The present work can also be used to determine the minimum number of experimental spectra that must be measured to extract all the information available from RIXS spectroscopy. In other words, from the finite number of fundamental spectra, we can generate the RIXS spectrum for arbitrary values of ϵ and ϵ_s.

A natural extension of this work, which is currently in progress, concerns the case of an electric-quadrupole approximation for the incoming photon combined with an electric-dipole approximation for the outgoing photon. This situation is relevant to many experiments on transition metals. Another perspective is to include the dipole–quadrupole interference term for the incoming photon, which gives rise to the XNCD effect in RIXS. For both cases, the simplification owing to symmetry is important because, in the absence of symmetry, 180 terms are involved in the dipole–quadrupole interference and 225 in the case of electric-quadrupole transitions. Another natural extension of this work would be to deal with magnetic groups [28,72].

Note added. Recently, Tagliavini and colleagues [72] submitted an article on similar subjects.

ACKNOWLEDGMENTS

We are very grateful to Coraline Letouzé and Hebatalla Elnaggar for fruitful discussions and comments.

DATA AVAILABILITY

The data that support the findings of this article are openly available [73].

APPENDIX: LIGAND FIELD MULTIPLET SIMULATIONS

Multiplet simulations of the $3d4f$ RIXS planes were carried out using Quanty Version 0.7 beta [74]. To emphasize the features, a slightly narrower broadening was used than that previously published for all simulations presented. Regarding $\mathrm{Ni^{II}}$ calculations, a 0-eV Gaussian broadening associated to

the experimental resolution was applied in addition to a 0.1-eV Lorentzian contribution. For all actinide simulations, a Lorentzian broadening of 3 eV and 0.5 eV for the $3d^9$ and $4f^{13}$ core-hole lifetimes, and a Gaussian broadening of 0.5 eV was implemented. As Quanty is semi-empirical, a modular Hamiltonian can be constructed consisting of a ligand field splitting (Ni: $3d$ orbitals/An: $5f$ orbitals), electron-electron interactions, and spin-orbit coupling in the initial, intermediate, and final electronic configurations of the respective RIXS processes, $2p3d$ RIXS for Ni^{II} and $3d4f$ RIXS for the actinides. A small magnetic field was applied on the z axis. The on-site energy of the $3d$ ligand field splitting for Ni^{II} [50] calculations and $5f$ ligand splitting [55,65] for all actinide calculations were the same as previously reported. All electron-electron interactions, associated to the Coulomb intershell repulsion and spin-exchange interactions, were scaled at 80% of the Hartree-Fock value. Spin-orbit coupling constants were kept at a scaling of 100%. No scaling has been applied regarding the intensity of the simulated RIXS maps.

[1] L. J. P. Ament, M. van Veenendaal, T. P. Devereaux, J. P. Hill, and J. van den Brink, Resonant inelastic x-ray scattering studies of elementary excitations, Rev. Mod. Phys. **83**, 705 (2011).

[2] F. M. F. de Groot, M. W. Haverkort, H. Elnaggar, A. Juhin, K.-J. Zhou, and P. Glatzel, Resonant inelastic x-ray scattering, Nat. Rev. Methods Primers **4**, 45 (2024).

[3] K. Ishii, S. Ishihara, Y. Murakami, K. Ikeuchi, K. Kuzushita, T. Inami, K. Ohwada, M. Yoshida, I. Jarrige, N. Tatami, S. Niioka, D. Bizen, Y. Ando, J. Mizuki, S. Maekawa, and Y. Endoh, Polarization-analyzed resonant inelastic x-ray scattering of the orbital excitations in $KCuF_3$, Phys. Rev. B **83**, 241101(R) (2011).

[4] M. Minola, G. Dellea, H. Gretarsson, Y. Peng, Y. Lu, J. Porras, T. Loew, F. Yakhou, N. Brookes, Y. Huang, J. Pelliciari, T. Schmitt, G. Ghiringhelli, B. Keimer, L. Braicovich, and M. Le Tacon, Collective nature of spin excitations in superconducting cuprates probed by resonant inelastic x-ray scattering, Phys. Rev. Lett. **114**, 217003 (2015).

[5] T. Inami, Magnetic circular dichroism in x-ray emission from ferromagnets, Phys. Rev. Lett. **119**, 137203 (2017).

[6] H. Elnaggar, P. Sainctavit, A. Juhin, S. Lafuerza, F. Wilhelm, A. Rogalev, M.-A. Arrio, C. Brouder, M. van der Linden, Z. Kakol, M. Sikora, M. W. Haverkort, P. Glatzel, and F. M. F. de Groot, Noncollinear ordering of the orbital magnetic moments in magnetite, Phys. Rev. Lett. **123**, 207201 (2019).

[7] N. B. Brookes, F. Yakhou-Harris, K. Kummer, A. Fondacaro, J. C. Cezar, D. Betto, E. Velez-Fort, A. Amorese, G. Ghiringhelli, L. Braicovich, *et al.*, The beamline ID32 at the ESRF for soft x-ray high energy resolution resonant inelastic x-ray scattering and polarisation dependent x-ray absorption spectroscopy, Nucl. Instrum. Methods Phys. Res. Sect. A **903**, 175 (2018).

[8] K.-J. Zhou, A. Walters, M. Garcia-Fernandez, T. Rice, M. Hand, A. Nag, J. Li, S. Agrestini, P. Garland, H. Wang, *et al.*, I21: An advanced high-resolution resonant inelastic x-ray scattering beamline at Diamond Light Source, J. Synchrotron Radiat. **29**, 563 (2022).

[9] S. Yamamoto, Y. Senba, T. Tanaka, H. Ohashi, T. Hirono, H. Kimura, M. Fujisawa, J. Miyawaki, A. Harasawa, T. Seike, *et al.*, New soft x-ray beamline BL07LSU at SPring-8, J. Synchrotron Radiat. **21**, 352 (2014).

[10] R. M. Jay, K. Kunnus, P. Wernet, and K. J. Gaffney, Capturing atom-specific electronic structural dynamics of transition-metal complexes with ultrafast soft x-ray spectroscopy, Annu. Rev. Phys. Chem. **73**, 187 (2022).

[11] G. E. Cutsail III and S. DeBeer, Challenges and opportunities for applications of advanced x-ray spectroscopy in catalysis research, ACS Catal. **12**, 5864 (2022).

[12] A. D. Rosa, G. Garbarino, J. E. Rodrigues, E. Mijit, J. Jacobs, D. Bugnazet, S. Pasternak, G. Berruyer, A. Moyne, C. Clavel, *et al.*, New opportunities for high pressure x-ray absorption spectroscopy at ID24-DCM and BM23 with the extremely brilliant source of the ESRF, High Press. Res. **44**, 248 (2024).

[13] D. Prieur, L. Amidani, E. F. Bazarkina, C. Hennig, E. Lawrence Bright, A. Rossberg, C. L. Silva, and K. O. Kvashnina, Frontiers of synchrotron methods for actinide science, Chem. Methods **5**, e202400073 (2025).

[14] K. O. Kvashnina and F. M. de Groot, Invisible structures in the x-ray absorption spectra of actinides, J. Electron Spectrosc. Relat. Phenom. **194**, 88 (2014).

[15] K. O. Kvashnina and S. M. Butorin, High-energy resolution x-ray spectroscopy at actinide $M_{4,5}$ and ligand K edges: What we know, what we want to know, and what we can know, Chem. Commun. **58**, 327 (2022).

[16] H. A. Kramers and W. Heisenberg, Über die streuung von strahlung durch atome, Z. Phys. **31**, 681 (1925).

[17] H. A. Kramers and W. Heisenberg, in *Master of Modern Physics*, edited by D. ter Haar, Princeton Series in Physics (Princeton University Press, Princeton, 1998), pp. 121–44.

[18] P. Glatzel and U. Bergmann, High resolution 1s core hole x-ray spectroscopy in 3d transition metal complexes–electronic and structural information, Coord. Chem. Rev. **249**, 65 (2005).

[19] J. J. Kas, J. J. Rehr, J. A. Soininen, and P. Glatzel, Real-space Green's function approach to resonant inelastic x-ray scattering, Phys. Rev. B **83**, 235114 (2011).

[20] D. Maganas, S. DeBeer, and F. Neese, A restricted open configuration interaction with singles method to calculate valence-to-core resonant x-ray emission spectra: A case study, Inorg. Chem. **56**, 11819 (2017).

[21] A. Juhin, C. Brouder, and F. de Groot, Angular dependence of resonant inelastic x-ray scattering: A spherical tensor expansion, Cent. Eur. J. Phys. **12**, 323 (2014).

[22] C. Brouder, Angular dependence of x-ray absorption spectra, J. Phys.: Condens. Matter **2**, 701 (1990).

[23] S. L. Altmann and P. Herzig, *Point Group Theory Tables* (Oxford University Press, Wien, 2011).

[24] C. Letouzé, G. Radtke, B. Lenz, and C. Brouder, Parametrization of the Coulomb interaction matrix with point-group symmetry, Phys. Rev. B **108**, 115137 (2023).

[25] E. Wigner, *Group Theory* (Academic Press, New York, 1959).

[26] S. Delhommaye, G. Radtke, C. Brouder, S. P. Collins, S. Huotari, C. Sahle, M. Lazzeri, L. Paulatto, and D. Cabaret, Assessing temperature effects on multipole contributions and angular dependence in core-level spectroscopies, Phys. Rev. B **104**, 024302 (2021).

[27] See Supplemental Material at http://link.aps.org/supplemental/10.1103/spng-p6c9 for the symmetry of relativistic cross sections, the N^G matrix for D_6, and the ligand field multiplet simulations of actinide $3d4f$ RIXS spectra, which includes Refs. [75–77].

[28] M. Furo, A. Hariki, and J. Kuneš, Theory of circular dichroism in resonant inelastic x-ray scattering, Phys. Rev. B **112**, 214429 (2025).

[29] C. Brouder, A. Juhin, A. Bordage, and M.-A. Arrio, Site symmetry and crystal symmetry: A spherical tensor analysis, J. Phys.: Condens. Matter **20**, 455205 (2008).

[30] B. T. Thole and G. van der Laan, Spin polarization and magnetic dichroism in photoemission from core and valence states in localized magnetic systems, Phys. Rev. B **44**, 12424 (1991).

[31] M. Sikora, A. Juhin, T.-C. Weng, P. Sainctavit, C. Detlefs, F. de Groot, and P. Glatzel, Strong K-edge magnetic circular dichroism observed in photon-in–photon-out spectroscopy, Phys. Rev. Lett. **105**, 037202 (2010).

[32] A. Hariki, K. Sakurai, T. Okauchi, and J. Kuneš, Separating altermagnetic and ferromagnetic effects in x-ray magnetic dichroism of rutile NiF_2, npj Quantum Mater. **10**, 49 (2025).

[33] A. Nag, G. S. Perren, H. Ueda, A. T. Boothroyd, D. Prabhakaran, M. García-Fernández, S. Agrestini, K.-J. Zhou, and U. Staub, Circular dichroism in resonant inelastic x-ray scattering from birefringence in CuO, Phys. Rev. Res. **7**, L022047 (2025).

[34] D. Takegami, T. Aoyama, T. Okauchi, T. Yamaguchi, S. Tippireddy, S. Agrestini, M. García-Fernández, T. Mizokawa, K. Ohgushi, K.-J. Zhou, J. Chaloupka, J. Kuneš, A. Hariki, and H. Suzuki, Circular dichroism in resonant inelastic x-ray scattering: Probing altermagnetic domains in MnTe, Phys. Rev. Lett. **135**, 196502 (2025).

[35] D. A. Varshalovich, A. N. Moskalev, and V. K. Khersonskii, *Quantum Theory of Angular Momentum* (World Scientific, Singapore, 1988).

[36] Y. I. Sirotine and M. P. Shaskolskaya, *Fundamentals of Crystal Physics* (Mir Publishers, Moscow, 1982).

[37] cryst.ehu.es.

[38] P. Azzi, R. Desmorat, B. Kolev, and F. Priziac, The distance to cubic symmetry class as a polynomial optimization problem, J. Elast. **156**, 157 (2024).

[39] J.-P. Serre, *Linear Representions of Finite Groups, Graduate Texts in Mathematics* (Springer, New York, 1977), Vol. 42.

[40] N. H. List, T. Saue, and P. Norman, Rotationally averaged linear absorption spectra beyond the electric-dipole approximation, Mol. Phys. **115**, 63 (2017).

[41] N. Bouldi, M. Mannini, M. Retegan, R. G. Miller, B. Cahier, P. Sainctavit, N. Guihéry, T. Mallah, D. Cabaret, D. Gouéré, *et al.*, XAS and XMCD reveal a Cobalt(II) imide undergoes high-pressure-induced spin crossover, J. Phys. Chem. C **126**, 5784 (2022).

[42] J. Yang, R. Dettori, J. P. F. Nunes, N. H. List, E. Biasin, M. Centurion, Z. Chen, A. A. Cordones, D. P. Deponte, T. F. Heinz, *et al.*, Direct observation of ultrafast hydrogen bond strengthening in liquid water, Nature (London) **596**, 531 (2021).

[43] K. Ishii, I. Jarrige, M. Yoshida, K. Ikeuchi, T. Inami, Y. Murakami, and J. Mizuki, Instrumental upgrades of the RIXS spectrometer at BL11XU at SPring-8, J. Electron Spectrosc. Relat. Phenom. **188**, 127 (2013).

[44] X. Gao, Development of polarization analysis of resonant inelastic x -ray scattering, Ph.D. thesis, Western Michigan University, Kalamazoo, 2013.

[45] L. Braicovich, M. Minola, G. Dellea, M. L. Tacon, M. M. Sala, C. Morawe, J.-C. Peffen, R. Supruangnet, F. Yakhou, G. Ghiringhelli, and N. B. Brookes, The simultaneous measurement of energy and linear polarization of the scattered radiation in resonant inelastic soft x-ray scattering, Rev. Sci. Instrum. **85**, 115104 (2014).

[46] J. Kim, D. Casa, A. Said, R. Krakora, B. J. Kim, E. Kasman, X. Huang, and T. Gog, Quartz-based flat-crystal resonant inelastic x-ray scattering spectrometer with sub-10 meV energy resolution, Sci. Rep. **8**, 1958 (2018).

[47] L. Manzanillas, J. Ablett, M. Choukroun, F. Iguaz, and J. Rueff, Development of an x-ray polarimeter at the SOLEIL synchrotron, Rev. Sci. Instrum. **95**, 053302 (2024).

[48] G. Ghiringhelli, M. Matsubara, C. Dallera, F. Fracassi, R. Gusmeroli, A. Piazzalunga, A. Tagliaferri, N. B. Brookes, A. Kotani, and L. Braicovich, NiO as a test case for high resolution resonant inelastic soft x-ray scattering, J. Phys.: Condens. Matter **17**, 5397 (2005).

[49] C. J. Ballhausen, *Introduction to Ligand Field Theory* (McGraw-Hill, New York, 1962).

[50] C.-Y. Liu, K. Ruotsalainen, K. Bauer, R. Decker, A. Pietzsch, and A. Föhlisch, Excited-state exchange interaction in NiO determined by high-resolution resonant inelastic x-ray scattering at the Ni $M_{2,3}$ edges, Phys. Rev. B **106**, 035104 (2022).

[51] G. Ghiringhelli, A. Piazzalunga, C. Dallera, T. Schmitt, V. N. Strocov, J. Schlappa, L. Patthey, X. Wang, H. Berger, and M. Grioni, Observation of two nondispersive magnetic excitations in NiO by resonant inelastic soft-x-ray scattering, Phys. Rev. Lett. **102**, 027401 (2009).

[52] T. Vitova, K. O. Kvashnina, G. Nocton, G. Sukharina, M. A. Denecke, S. M. Butorin, M. Mazzanti, R. Caciuffo, A. Soldatov, T. Behrends, and H. Geckeis, High energy resolution x-ray absorption spectroscopy study of uranium in varying valence states, Phys. Rev. B **82**, 235118 (2010).

[53] K. O. Kvashnina, S. M. Butorin, P. Martin, and P. Glatzel, Chemical state of complex uranium oxides, Phys. Rev. Lett. **111**, 253002 (2013).

[54] K. O. Kvashnina, H. C. Walker, N. Magnani, G. H. Lander, and R. Caciuffo, Resonant x-ray spectroscopy of uranium intermetallics at the $M_{4,5}$- edges of uranium, Phys. Rev. B **95**, 245103 (2017).

[55] L. Amidani, M. Retegan, A. Volkova, K. Popa, P. M. Martin, and K. O. Kvashnina, Probing the local coordination of hexavalent uranium and the splitting of $5f$ orbitals induced by chemical bonding, Inorg. Chem. **60**, 16286 (2021).

[56] S. M. Butorin, A. Modin, J. R. Vegelius, K. O. Kvashnina, and D. K. Shuh, Probing chemical bonding in uranium dioxide by means of high-resolution x-ray absorption spectroscopy, J. Phys. Chem. C **120**, 29397 (2016).

[57] S. M. Butorin, K. O. Kvashnina, A. L. Smith, K. Popa, and P. M. Martin, Crystal-field and covalency effects in uranates: An x-ray spectroscopic study, Chem. Eur. J. **22**, 9693 (2016).

[58] R. Bes, M. Rivenet, P. L. Solari, K. O. Kvashnina, A. C. Scheinost, and P. M. Martin, Use of HERFD-XANES at the U L_3- and M_4- edges to determine the uranium valence state on $[Ni(H_2O)_4]_3[U(OH,H_2O)(UO_2)_8O_{12}(OH)_3]$, Inorg. Chem. **55**, 4260 (2016).

[59] K. Kvashnina, Y. Kvashnin, and S. Butorin, Role of resonant inelastic x-ray scattering in high-resolution core-level spectroscopy of actinide materials, J. Electron Spectrosc. Relat. Phenom. **194**, 27 (2014).

[60] T. Vitova, I. Pidchenko, D. Fellhauer, P. S. Bagus, Y. Joly, T. Pruessmann, S. Bahl, E. Gonzalez-Robles, J. Rothe, M. Altmaier, M. A. Denecke, and H. Geckeis, The role of the 5f valence orbitals of early actinides in chemical bonding, Nat. Commun. **8**, 16053 (2017).

[61] E. Epifano, M. Naji, D. Manara, A. C. Scheinost, C. Hennig, J. Lechelle, R. J. Konings, C. Guéneau, D. Prieur, T. Vitova, *et al.*, Extreme multi-valence states in mixed actinide oxides, Commun. Chem. **2**, 59 (2019).

[62] T. G. Burrow, N. M. Alcock, M. S. Huzan, M. A. Dunstan, J. A. Seed, B. Detlefs, P. Glatzel, M. O. J. Y. Hunault, J. Bendix, K. S. Pedersen, and M. L. Baker, Determination of uranium central-field covalency with 3d4f resonant inelastic x-ray scattering, J. Am. Chem. Soc. **146**, 22570 (2024).

[63] T. G. Burrow, N. M. Alcock, M. S. Huzan, M. A. Dunstan, J. A. Seed, B. Detlefs, P. Glatzel, M. O. J. Y. Hunault, J. Bendix, K. S. Pedersen, and M. L. Baker, Correction to "Determination of uranium central-field covalency with 3d4f resonant inelastic x-ray scattering", J. Am. Chem. Soc. **147**, 37876 (2025).

[64] B. Schacherl, M. Tagliavini, H. Kaufmann-Heimeshoff, J. Göttlicher, M. Mazzanti, K. Popa, O. Walter, T. Pruessmann, C. Vollmer, A. Beck, *et al.*, Resonant inelastic x-ray scattering tools to count 5f electrons of actinides and probe bond covalency, Nat. Commun. **16**, 1221 (2025).

[65] S. M. Butorin, 3d-4f resonant inelastic x-ray scattering of actinide dioxides: Crystal-field multiplet description, Inorg. Chem. **59**, 16251 (2020).

[66] A. C. Scheinost, J. Claussner, J. Exner, M. Feig, S. Findeisen, C. Hennig, K. O. Kvashnina, D. Naudet, D. Prieur, A. Rossberg, M. Schmidt, *et al.*, ROBL-II at ESRF: A synchrotron toolbox for actinide research, J. Synchrotron Radiat. **28**, 333 (2021).

[67] J. M. Ablett, A. Berlioux, D. Prieur, J. Harrison, L. Heller, S. Gliga, and J.-P. Rueff, MULTIXS: A new scanning multi-analyzer x-ray emission spectrometer at the GALAXIES beamline at synchrotron SOLEIL, Rev. Sci. Instrum. **96**, 053104 (2025).

[68] M. Moretti Sala, K. Martel, C. Henriquet, A. Al Zein, L. Simonelli, C. J. Sahle, H. Gonzalez, M.-C. Lagier, C. Ponchut, S. Huotari, *et al.*, A high-energy-resolution resonant inelastic x-ray scattering spectrometer at ID20 of the European synchrotron radiation facility, J. Synchrotron Radiat. **25**, 580 (2018).

[69] P. Glatzel, A. Harris, P. Marion, M. Sikora, T.-C. Weng, C. Guilloud, S. Lafuerza, M. Rovezzi, B. Detlefs, and L. Ducotté, The five-analyzer point-to-point scanning crystal spectrometer at ESRF ID26, J. Synchrotron Radiat. **28**, 362 (2021).

[70] A. Zimina, K. Dardenne, M. A. Denecke, D. E. Doronkin, E. Huttel, H. Lichtenberg, S. Mangold, T. Pruessmann, J. Rothe, T. Spangenberg, *et al.*, CAT-ACT—A new highly versatile x-ray spectroscopy beamline for catalysis and radionuclide science at the KIT synchrotron light facility ANKA, Rev. Sci. Instrum. **88**, 113113 (2017).

[71] D. W. Lynch and R. D. Cowan, Effect of hybridization on 4d → 4f spectra in light lanthanides, Phys. Rev. B **36**, 9228 (1987).

[72] M. Tagliavini, F. Wenzel, and M. W. Haverkort, Polarization dependency in resonant inelastic x-ray scattering, arXiv:2510.12891.

[73] T. G. Burrow, Angular dependence and powder average of resonant inelastic x-ray scattering [Data set], Zenodo (2025), https://doi.org/10.5281/zenodo.18462687.

[74] M. W. Haverkort, Quanty for core level spectroscopy - excitons, resonances and band excitations in time and frequency domain, J. Phys.: Conf. Ser. **712**, 012001 (2016).

[75] L. C. Biedenharn and J. D. Louck, *Angular Momentum in Quantum Physics*, Encyclopedia of Mathematics and its Applications, Vol. 8 (Addison-Wesley, Reading, 1981).

[76] C. Itzykson and J.-B. Zuber, *Quantum Field Theory* (McGraw-Hill, New York, 1980).

[77] N. Bouldi and C. Brouder, Gauge invariance and relativistic effects in photon absorption and scattering by matter, Eur. Phys. J. B **90**, 246 (2017).